Computational Mechanics (1989) 5, 375–400

Computational Mechanics

© Springer-Verlag 1989

On continuum damage-elastoplasticity at finite strains

A computational framework

J. C. Simo
Stanford University, Durand Building, Stanford, CA 94305-4040, USA

J. W. Ju
Department of Civil Engineering and Operations Research, Princeton University, Princeton, NJ 08544, USA

Abstract. A strain-based continuum damage-elastoplasticity formulation at finite strains is proposed based on an additive split of the *stress* tensor. Within the proposed framework, a hyperelastic extension of the classical J_2-flow theory is developed as a model problem, with a rate-free formulation of the (linear) kinematic hardening law that is free from spurious stress oscillation in the simple shear test. The algorithmic implementation of the coupled damage-elastoplasticity model is shown to reduce to a trivial modification of the classical radial return which is amenable to *exact* linearization. This results in a closed form expression for the *consistent* elastoplastic-damage modulus. The algorithmic treatment of the damage model with no restrictions on the functional forms governing the plastic response is considered subsequently. It is emphasized that objective rates and incrementally objective algorithms play no role in the present approach. A number of numerical experiments are presented that illustrate the performance of the proposed formulation.

1 Introduction

A continuum strain-based damage formulation coupled with elastoplasticity at finite strains is proposed within the framework of a stress split. The proposed formulation is a natural extension of the infinitesimal continuum damage-elastoplasticity model previously developed in Simo and Ju (1987a, b). The damage model is based on the effective stress concept and linked to the history of total strains. The strain-based characterization of damage is particularly well suited for large scale computation.

Coupling of continuum damage with elastoplasticity is considered in detail. The stress tensor is decomposed into an initial and a plastic relaxation parts. We note that this is a mathematically sound operation since, as opposed to the strain tensors which are nonlinear functions of the configurations, stress tensors are elements of a vector space (the cotangent space at a given configuration). Stresses and strain rates (not strains) are conjugate variables; the duality pairing being the stress power. Although formulations based on the multiplicative decomposition appear to be significantly better conditioned for large strains (Simo 1988b, c), the present approach has the advantage of providing a framework in which damage is trivially accommodated. It should also be kept in mind that in the presence of damage degradation, very large strains are unlikely to develop.

In addition to providing a convenient framework for the incorporation of continuum damage degradation, some noteworthy features of the proposed approach are the following.

(1) For the particular J_2-plasticity considered, the kinematic hardening law is formulated without resorting to objective rates. Interestingly, the proposed rate-free generalization of the Prager-Ziegler model results in a linear relation between the true stress and the amount of shear in the simple shear test with kinematic hardening. Hence, the formulation avoids spurious oscillatory stress responses typically associated with hypoelastic formulations employing the Jaumann time derivative (e.g., Nagtegaal and de Jong 1981b).

(2) The elastic response is truly hyperelastic. From a computational standpoint, this enables one to entirely bypass the need to integrate hypoelastic constitutive equations, see also Simo and Ortiz (1985), and Simo (1988b, c)

(3) As in the strain-based (infinitesimal) formulation considered in Simo and Ju (1987a, b),

continuum degradation is characterized on the basis of the strain energy norm of the total strain tensor. The alternative assumption that the amount of damage present in the material is associated with the energy norm of the elastic strain tensor (and not the total strain tensor) would be equivalent to postulating that damage and plasticity mechanisms are entirely uncoupled. This however, is not the case from a physical standpoint. As an example of this coupling, we recall that in fracture mechanics the so-called "plastic correction" for the effective crack length is typically performed when considering elastoplastic crack growth and crack stability (e.g. Knott 1973). Furthermore, we note that some recently proposed damage models (e.g., Lemaitre 1984) neglect altogether the effect of elastic strains in damage evolution on the grounds that total and plastic strains are approximately equal in the finite deformation range.

An outline of the remaining of this paper is as follows. The local elastoplastic-damage constitutive equations of evolution are derived in Sect. 2. Both spatial (Eulerian) and material (Lagrangian) descriptions are discussed. By temporarily ignoring the damage part, a hyperelastic formulation of the classical J_2-flow theory is presented in Sect. 3 as a specific model problem. Computational aspects involved in the numerical integration of this particular model, as well as in the general case involving plasticity and damage, are presented in Sect. 4. Numerical examples including damage coupled with plastic flow are discussed in Sect. 5. This set of numerical simulations represents an effort towards the development of a comprehensive computational benchmark for finite strain elastoplastic formulations. The examples have been taken from different sources in the recent literature and are documented as to facilitate comparison with other formulations.

We emphasize once more that the presence of damage typically limits the magnitude of the strains, the proposed approach is not intended to be applicable to finite deformation elastoplasticity involving very large strains. For this class of truly finite strain problems, a multiplicative decomposition of the deformation gradient is in fact more suitable (Simo 1988 b, c). Nevertheless, the proposed approach exhibits good performance in the benchmark problems for plasticity at finite strains considered in Sect. 5.

2 Evolution equations of damage coupled with elastoplasticity

A basic feature of the proposed strain-based constitutive model is an additive split of the stress tensor into the initial elastic and plastic relaxation parts. Such a split enables one to incorporate a simple strain-based continuum damage model capable of predicting so-called splitting modes (see also Ortiz 1985). Additive splits of the stress tensor has been proposed in Simo (1986) for finite strain viscoelasticity, and in Simo and Ju (1987 a, b) for infinitesimal damage-elastoplasticity.

The present approach, which is based on the missing notions of effective stress (as proposed by Kachanov 1958) and the hypothesis of strain equivalence, is the finite strain version of the formulation proposed in Simo and Ju (1987 a, b). The account that follows employs a material description. An entirely equivalent formulation can be made in the spatial description (often favored in treatments of elastoplasticity) and is outlined in Remarks.

2.1 Thermodynamic basis. Stress split

Let $\mathbf{S}$ be the symmetric Piola-Kirchhoff stress tensor. We consider a free energy potential $\Psi(\mathbf{C}, \mathbf{S}^p, \mathbf{Q}, d)$ of the following form

$$\Psi(\mathbf{C}, \mathbf{S}^p, \mathbf{Q}, d) := (1-d)\,\Psi^0(\mathbf{C}) - \mathbf{E}:\mathbf{S}^p + \Xi(\mathbf{Q}, \mathbf{S}^p) \tag{2.1}$$

Here $\mathbf{E} := 1/2\,[\mathbf{C} - \mathbf{1}]$ denotes the Lagrangian strain tensor, with $\mathbf{C} := \mathbf{F}^T\mathbf{F}$, where $\mathbf{F}$ is the deformation gradient, and $\mathbf{S}^p$ is an internal plastic variable referred to as plastic relaxation stress tensor in what follows. In addition, d denotes the damage parameter, $\mathbf{q}$ is a suitable set of plastic variables, ψ^o is the stored energy function for a virgin material and Ξ denotes a plastic potential function.

Within the framework of the purely mechanical theory, the Clausius-Duhem inequality reduces to

$$-\varrho_{\text{ref}}\dot{\Psi} + \mathbf{S}:\dot{\mathbf{E}} \geq 0, \tag{2.2}$$

where ϱ_{ref} is the mass density in the reference configuration. Standard procedures [Coleman and Gurtin (1967)] then yield

$$\mathbf{S} = (1-d)\,\varrho_{\text{ref}}\frac{\partial \Psi^o(\mathbf{E})}{\partial \mathbf{E}} - \mathbf{S}^p, \tag{2.3}$$

together with the dissipative inequalities

$$\varrho_{\text{ref}}\Psi^o\,\dot{d} \geq 0 \quad \text{and} \quad -\varrho_{\text{ref}}\frac{\partial \Xi}{\partial \mathbf{Q}}\cdot\dot{\mathbf{Q}} - (\varrho_{\text{ref}}\frac{\partial \Xi}{\partial \mathbf{S}^p} - \mathbf{E}):\dot{\mathbf{S}}^p \geq 0\,. \tag{2.4}$$

Accordingly, from (2.3) one obtains an additive split of the stress tensor in which $[(1-d)\,\varrho_{\text{ref}}\partial\Psi^o(\mathbf{E})/\partial\mathbf{E}]$ and $\mathbf{S}^p$ are referred to as the elastic-damage and plastic relaxation stress tensors, respectively. For convenience, we introduce the following notation

$$\mathbf{S}^o := \varrho_{\text{ref}}\frac{\partial \Psi^o(\mathbf{E})}{\partial \mathbf{E}}, \tag{2.5}$$

and we refer to $\mathbf{S}^0$ as the initial (undamaged) elastic stress tensor. It also follows from (2.4) that the thermodynamic flux conjugate to the damage variable d is simply $\Psi^o(\mathbf{E})$.

Remark 2.1. The spatial counterpart of the material description outlined above can be obtained by employing standard push-forward operations with the deformation gradients. For instance, the spatial counterpart of (2.3) reads

$$\boldsymbol{\tau} = (1-d)\,\boldsymbol{\tau}^o - \boldsymbol{\tau}^p, \qquad \boldsymbol{\tau}^o = \varrho_{\text{ref}}\frac{\partial \bar{\Psi}^o(\mathbf{e},\mathbf{F})}{\partial \mathbf{e}} \tag{2.6}$$

Here $\bar{\Psi}^o$ is the stored energy function in terms of the Eulerian strain and the deformation gradient. Relation $(2.6)_2$ is an alternative statement (in terms of strain rather than metric tensors) of the so-called Doyle-Ericksen formula which plays a central role in elasticity; see Marsden and Hughes (1983) and Simo and Marsden (1984). □

Remark 2.2. Observe that the plastic strain (either $\mathbf{E}^p$ in the material description or $\mathbf{e}^p$ in the spatial description) may be defined as the residual strain obtained by means of a local unloading. To see this, let $\mathbf{S}^o = \varrho_{\text{ref}}\partial\bar{\Psi}^o(\mathbf{E})/\partial\mathbf{E} := \boldsymbol{\Gamma}(\mathbf{E})$. Assuming that $\boldsymbol{\Gamma}$ invertible (at least locally), from (2.3) we obtain, by definition,

$$\mathbf{0} = (1-d)\,\boldsymbol{\Gamma}(\mathbf{E}^p) - \mathbf{S}^p \Rightarrow \mathbf{E}^p := \boldsymbol{\Gamma}^{-1}(\bar{\mathbf{S}}^p) \tag{2.7}$$

where we have set $\bar{\mathbf{S}}^p := \mathbf{S}^p/(1-d)$. In the spatial description, we have $\mathbf{e}^p = \mathbf{F}\,\mathbf{E}^p\,\mathbf{F}^T$. □

2.2 *Characterization of damage. Elastic-damage modulus*

In this Section, we describe the strain-based characterization of damage at finite strains in the spirit of Kachanov (1958), by means of an isotropic damage mechanism. We define the equivalent measure τ in material description by the expression

$$\tau := \sqrt{2\Psi^o(\mathbf{E})} \tag{2.8}$$

A damage criterion in strain space is then introduced by requiring that at any time t

$$g(\bar{\tau}_t, r_t) := \bar{\tau}_t - r_t \leq 0, \qquad t \in \mathbb{R}_+\,. \tag{2.9}$$

Damage evolution equations and the damage loading/unloading conditions are defined by the relations

$$\dot{d}_t = \dot{\lambda}\,H(d_t, \bar{\tau}_t) \quad \text{and} \quad \dot{r}_t = \dot{\lambda} \tag{2.10}$$

where the irreversible nature of damage is captured by enforcing that the function $\dot{\lambda}$ satisfy the (Kuhn-Trucker) unilateral restrictions

$$\dot{\lambda} \geq 0, \quad g(\bar{\tau}_t, r_t) \leq 0, \quad \dot{\lambda} g(\bar{\tau}_t, r_t) = 0 \tag{2.11}$$

One can show that these conditions are in fact optimality conditions for a principle of maximum damage dissipation (Simo and Ju 1987 a, b). From a damage consistency condition entirely analogous to that typically employed in the rate-independent plasticity, one determines $\dot{\lambda}$ and r_t by enforcing that during the damage loading

$$g(\bar{\tau}_t, r_t) = \dot{g}(\bar{\tau}_t, r_t) = 0 \Rightarrow \dot{\lambda} = < \dot{\tau}_t > \tag{2.12}$$

so that

$$r_t = \max\{r_0, \max_{s \in (-\infty, t)} \bar{\tau}_s\} \tag{2.13}$$

where $< \bullet >$ is the McAuley bracket. A spatial version of the above characterization of damage can be carried out in exactly the same manner.

2.2.1 Elastic-damage tangent modulus

In the absence of further plastic flow, the relation between strain rate and stress rate is obtained as follows. In a (damage) loading process

$$\dot{\mathbf{S}} = (1-d)\,\dot{\mathbf{S}}^o - H(\bar{\tau}, d)\,\dot{\tau}\,\mathbf{S}^o = (1-d)\,\varrho_{\text{ref}} \frac{\partial^2 \Psi^o}{\partial \mathbf{E}^2} : \dot{\mathbf{E}} - H(\bar{\tau}, d)\,\dot{\tau}\,\mathbf{S}^o \tag{2.14}$$

Thus, since $\dot{\tau} = 1/\tau \mathbf{S}^o : \dot{\mathbf{E}}$, we obtain $\dot{\mathbf{S}} = \mathbf{A}(\mathbf{E}, d) : \mathbf{E}$, where $\mathbf{A}(\mathbf{E}, d)$ is a symmetric rank four tensor referred to as the elastic-damage tangent modulus at finite strain, and given by

$$\mathbf{A}(\mathbf{E}, d) = (1-d) \frac{\partial^2 \Psi^o}{\partial \mathbf{E}^2} - \frac{H}{\tau} \mathbf{S}^o \otimes \mathbf{S}^o \tag{2.15}$$

On speaks of $\mathbf{A}^o(\mathbf{E}) := \varrho_{\text{ref}} \partial^2 \Psi^o(\mathbf{E}) / \partial \mathbf{E}^2$ as the initial (undamaged) material elasticity tensor. The expression for the elastic-damage modulus in the spatial description follows at once from (2.15) by a push-forward operation, and is recorded in Box 1 along with a summary of the damage model.

Remark 2.3. [Viscous regularized damage model]. The damage model outlined above is rate independent. Typically, in the softening regime, lack of uniqueness will arise if such an approach is employed. A possible appraoch is to regularize this model by introducing a viscous dependency analogous to that employed in viscoplasticity. Accordingly, one replaces the damage evolution (2.10) with the rate-dependent model. (BOX 1 und 1 a)
In the functional analysis literature, such a regularization often goes by the name of Yosida regularization (Pazy 1983, page 9). □

We now proceed to characterize the plastic response by defining the evolution of the effective plastic relaxation stress τ^p.

2.3 Characterization of plastic response. Tangent modulus

Within the proposed framework, plastic response is characterized in the so-called effective stress space in terms of the the effective stress. We refer to Simo and Ju (1987 a) for a discussion of these notions.

2.3.1 Yield condition

In the spatial description, one assumes a yield condition that depends on the current effective stress $\bar{\tau}$ and a suitable set of internal plastic variables $\mathbf{q}$ the evolution of which is defined below. Since this

Box 1. Isotropic rate-independent elastic-damage at finite strain

Spatial	Material (convected)
(i) Additive split of the effective stress:	
$\bar{\tau} = \varrho_{\text{ref}} \frac{\partial \Psi^o(\mathbf{e},\mathbf{F})}{\partial \mathbf{e}} - \bar{\tau}^p$	$\bar{\mathbf{S}} = \varrho_{\text{ref}} \frac{\partial \Psi^o(\mathbf{E})}{\partial \mathbf{E}} - \bar{\mathbf{S}}^p$
$\tau = (1-d)\bar{\tau}$	$\mathbf{S} = (1-d)\mathbf{S}$
$\tau^p = (1-d)\tau^p$	$\mathbf{S}^p = (1-d)\bar{\mathbf{S}}^p$
(ii) Damage evolution:	
$\bar{\tau} := \sqrt{2\varrho_{\text{ref}}\Psi^o(\mathbf{e},\mathbf{F})} := \sqrt{2\varrho_{\text{ref}}\Psi^o(\mathbf{E})}$	
$\dot{d} = \dot{\lambda} H(\bar{\tau}, d); \quad \dot{\lambda} \geq 0$	
$g := \bar{\tau} - r_t \leq 0; \quad \dot{\lambda} g = 0$	
(iii) Elastic-damage modulus; (similar in a material description)	
$\mathbf{a} := (1-d)\varrho_{\text{ref}} \frac{\partial^2 \Psi^o}{\partial \mathbf{e}^2} - \frac{H}{\tau} \tau^o \otimes \tau^o$	
(iv) Plasticity: see Box 2	

Box 1a. Viscous rate-dependent elastic-damage model

$$\dot{d}_t = \mu < g(\bar{\tau}_t, r_t) > H(\bar{\tau}_t, d_t)$$
$$\dot{r}_t = \mu < g(\bar{\tau}_t, r_t) >$$

function may depend on $\bar{\tau}$ through its invariants or its deviator one needs to include explicitly the dependence on the spatial metric tensor, denoted by $\mathbf{g}$[1]. Accordingly, one writes

$$\phi(\bar{\tau}, \mathbf{g}, \mathbf{q}) \leq 0 \tag{2.16}$$

One could also define the yield condition entirely in strain space by postulating at the outset the form $\bar{\phi}(\mathbf{g}, \tau^p, \mathbf{q}, \mathbf{F}) \leq 0$. Alternatively, one may think of this strain space form as emanating from (2.16) through the stress-strain relations, i.e.,

$$\bar{\phi}(\mathbf{g}, \bar{\tau}^p, \mathbf{q}, \mathbf{F}) := \phi(2\varrho_{\text{ref}} \frac{\partial \Psi^o(\mathbf{g},\mathbf{F})}{\partial \mathbf{g}} - \bar{\tau}^p, \mathbf{q}). \tag{2.17}$$

In the material description, one can show that the most general form of yield condition which is consistent with material frame indifference takes the form

$$\bar{\Phi}(\mathbf{E}, \bar{\mathbf{S}}^p, \mathbf{Q}) \leq 0, \tag{2.18}$$

where $\mathbf{Q} := \boldsymbol{\phi}^* \mathbf{q}$ is the pull-back of $\mathbf{q}$. It should be noted that (2.18) does not preclude anisotropic response. Material frame indifference, on the other hand, necessarily implies that the spatial function given by Eq. (2.16) must be isotropic.

1 This dependence on $\mathbf{g}$ is, in fact, essential and constitutes the basis for a covariant formulation (Marsden and Hughes 1983)

2.3.2 Flow rule and hardening law

Although more general formulations are possible, we shall restrict our attention to the case of an associative flow rule. Accordingly, we assume an evolution equation for $\mathbf{S}^p$ of the form

$$\dot{\mathbf{S}}^p = \dot{\gamma}\,\frac{\partial \bar{\Phi}(\mathbf{E}, \bar{\mathbf{S}}^p, \mathbf{Q})}{\partial \mathbf{E}}. \tag{2.19}$$

Here, γ is a plastic consistency parameter that determines the irreversible nature of the plastic flow according to the Kuhn-Trucker conditions

$$\dot{\gamma} \geq 0, \quad \bar{\Phi}(\mathbf{E}, \bar{\mathbf{S}}^p, \mathbf{Q}) \leq 0, \quad \dot{\gamma}\bar{\Phi}(\mathbf{E}, \bar{\mathbf{S}}^p, \mathbf{Q}) := 0 \tag{2.20}$$

The characterization of the elastoplastic response is completed by prescribing the evolution of the internal (plastic) state variable $\mathbf{Q}$ according to a rate equation of the form $\dot{\mathbf{Q}} = \dot{\gamma}\mathbf{H}(\mathbf{E}, \bar{\mathbf{S}}^p, \mathbf{Q})$. One refers to the function $\mathbf{H}$ as the generalized hardening modulus.

Remark 2.4. (Viscoplasticity). The formulation outlined above readily extends to the case of viscoplasticity. The plastic flow rule and the hardening law take the same functional forms as before with $\dot{\gamma}$ now replaced by $f(\bar{\Phi})/\eta$, where η is the viscosity coefficient and $f(\bar{\Phi})$ is the viscoplastic flow function depending on $\bar{\Phi}$. It can be shown that as $\eta \to 0$ one recoverse the rate-independent plasticity limit. □

2.3.3 Elastoplastic-damage tangent modulus

The plastic consistency parameter γ is determined by enforcing the so-called plastic consistency condition. Explicitly, upon loading ($\dot{\gamma} > 0$) one must have $\bar{\Phi}(\mathbf{E}, \bar{\mathbf{S}}^p, \mathbf{Q}) = 0$ and $\dot{\bar{\Phi}}(\mathbf{E}, \bar{\mathbf{S}}^p, \mathbf{Q}) = 0$. Direct application of the chain rule and use of the flow rule yield the following expression for γ:

$$\dot{\gamma} = \left[\frac{\partial \bar{\Phi}}{\partial \mathbf{E}} : \dot{\mathbf{E}}\right] \Big/ \left[\frac{\partial \bar{\Phi}}{\partial \mathbf{E}} : \frac{\partial \bar{\Phi}}{\partial \bar{\mathbf{S}}^p} - \frac{\partial \bar{\Phi}}{\partial \mathbf{Q}} \cdot \mathbf{H}\right]. \tag{2.21}$$

By inserting (2.21) into the flow rule (2.19) and using the rate form of (2.3), we obtain $\dot{\mathbf{S}} = \mathbf{A}^{ep} : \dot{\mathbf{E}}$, where $\bar{\mathbf{A}}^{ep}$ is the effective elastoplastic tangent modulus given by

$$\bar{\mathbf{A}}^{ep} := \mathbf{A}^o - \frac{\dfrac{\partial \bar{\Phi}}{\partial \mathbf{E}} \otimes \dfrac{\partial \bar{\Phi}}{\partial \mathbf{E}}}{\dfrac{\partial \bar{\Phi}}{\partial \bar{\mathbf{S}}^p} : \dfrac{\partial \bar{\Phi}}{\partial \mathbf{E}} - \dfrac{\partial \bar{\Phi}}{\partial \mathbf{Q}} \cdot \mathbf{H}} \tag{2.22}$$

Finally, since $\mathbf{S} = (1 - d)\bar{\mathbf{S}}$, from (2.22), (2.10) and the relation $\bar{\tau} = \mathbf{S}^o : \dot{\mathbf{E}}/\bar{\tau}$, we obtain $\dot{\mathbf{S}} = \mathbf{A}^{ep} : \mathbf{d}$. Here $\mathbf{A}^{ep}$ is the elastoplastic-damage tangent modulus given by

$$\mathbf{A}^{ep} := (1 - d)\bar{\mathbf{A}}^{ep} - \frac{H}{\bar{\tau}}\bar{\mathbf{S}} \otimes \mathbf{S}^o \tag{2.23}$$

For easy reference, basic equations derived in this section have been summarized in Boxes 1 and 2. Here, $L_v\bar{\tau}^p$ denotes the Lie derivative of the spatial contravariant tensor τ^p which is define by the relation

$$L_v\bar{\tau}^p := \mathbf{F}\dot{\mathbf{S}}^p\,\mathbf{F}^T \tag{2.24}$$

For a general definition of the Lie derivative we refer to Marsden and Hughes (1983, Sec. 1.6).

3 A hyperelastic formulation of classical J_2-flow theory

The following features characterize the hyperelastic formulation of the classical J_2-flow theory outlined below (Box 2).

(i) The elastic response is truly hyperelastic. In the absence of plastic flow, the response of the constitutive model is that of a polyconvex Hadamard material.

(ii) Volumetric and deviatoric responses are exactly uncoupled for any range of deformations. In fact, the proposed model predicts zero hydrostatic pressure in a simple shear test.

(iii) The kinematic hardening rule is formulated without resorting to objective rates. Within the context of a linear kinematic hardening law of the Prager-Ziegler type, the back stress – as defined below – is simply a fraction of the plastic stress τ^p.

(iv) In a simple shear test, the proposed rate-free characterization of kinematic hardening leads to a linear relation between the true shear stress and the amount of shear deformation. Spurious oscillations associated with the Jaumann derivative in classical rate formulations of the kinematic hardening, as first documented by Nagtegaal and de Jong (1981 b), are thus avoided.

Box 2. Strain-based elastoplastic model in effective stress space

Spatial	Material (convected)
(i) Additive stress split:	
$\bar{\tau} = \bar{\tau}^o - \bar{\tau}^p$	$\bar{\mathbf{S}} = \bar{\mathbf{S}}^0 - \bar{\mathbf{S}}^p$
(ii) Initial elastic stress from the hyperelastic potential:	
$\bar{\tau}^o = \varrho_{\text{ref}} \dfrac{\partial \psi^o(\mathbf{e}, \mathbf{F})}{\partial \mathbf{e}}$	$\bar{\mathbf{S}}^o = \varrho_{\text{ref}} \dfrac{\partial \Psi^o(\mathbf{E})}{\partial \mathbf{E}}$
(iii) Plastic flow rule:	
$\mathbf{L}_v \bar{\tau}^p = \dot{\gamma} \dfrac{\partial \bar{\phi}}{\partial \mathbf{e}} (\mathbf{e}, \bar{\tau}^p, \mathbf{q}, \mathbf{F})$	$\bar{\mathbf{S}} = \dot{\gamma} \dfrac{\partial \bar{\Phi}}{\partial \mathbf{E}} (\mathbf{E}, \bar{\mathbf{S}}^p, \mathbf{Q})$
(iv) Hardening law:	
$L_v \mathbf{q} = \dot{\gamma} \mathbf{h}(\mathbf{e}, \bar{\tau}^p, \mathbf{q}, \mathbf{F})$	$\dot{\mathbf{Q}} = \dot{\gamma} \mathbf{H}(\mathbf{E}, \bar{\mathbf{S}}^p, \mathbf{Q})$
(v) Loading/unloading conditions:	
$\dot{\gamma} \geq 0, \quad \bar{\phi} \leq 0$	$\dot{\gamma} \geq 0, \quad \bar{\Phi} \leq 0$
$\dot{\gamma} \bar{\phi} = 0$	$\dot{\gamma} \bar{\Phi} = 0$
(vi) Spatial elastoplastic modulus (analogous in a material setting):	
$\bar{\mathbf{a}}^{ep} = \mathbf{a}^o + \dfrac{\dfrac{\partial \bar{\phi}}{\partial \mathbf{e}} \otimes \dfrac{\partial \bar{\phi}}{\partial \mathbf{e}}}{\dfrac{\partial \bar{\phi}}{\partial \tau^p} : \dfrac{\partial \bar{\phi}}{\partial \mathbf{e}} - \dfrac{\partial \bar{\phi}}{\partial \mathbf{q}} \cdot \mathbf{h}}$	
(vii) Spatial elastoplastic-damage modulus:	
$\mathbf{a}^{epd} := (1-d)\bar{\mathbf{a}}^{ep} - \bar{\tau} \otimes \tau^0$	

3.1 Elastic response. Uncoupled volumetric/deviatoric response

Completely uncoupled volumetric/deviatoric response throughout the entire range of deformation – a basic feature of the proposed approach – is achieved through a multiplictive decomposition of the deformation gradient. Our treatment follows Simo, Taylor and Pister (1985), and Simo (1986).

The volumetric/deviatoric multiplicative decomposition goes back at least to Flory (1961) for the isotropic case. Denoting by $J := \det \mathbf{F}$ the Jacobian determinant of the deformation gradient, one introduces the multiplicative split

$$\mathbf{F} = J^{1/3}\bar{\mathbf{F}}, \quad \text{where} \quad \bar{\mathbf{F}} := J^{-1/3}\mathbf{F}. \tag{3.1}$$

Here, $\bar{\mathbf{F}}$ is the volume preserving part of $\mathbf{F}$ since $\det \bar{\mathbf{F}} := 1$. One may also define the volume-preserving right Cauchy-Green and Lagrange strain tensors as

$$\bar{\mathbf{C}} = J^{-2/3}\mathbf{C} := \bar{\mathbf{F}}^T\mathbf{F}, \quad \bar{\mathbf{E}} := \frac{1}{2}[\bar{\mathbf{C}} - \mathbf{1}], \tag{3.2}$$

where $\mathbf{1}$ is the unit rank-two tensor.

3.1.1 Specific elastic model

The following poly-convex hyperelastic model, previously considered in Simo (1986), will be employed in what follows. We emphasize that in the subsequent development the stresses τ, τ^p, $\mathbf{S}$, and $\mathbf{S}^p$ should be interpreted as effective stresses. To alleviate the notation, however, and to avoid confusion with the volume preserving quantities, the superposed bar will be omitted.

$$\tau := JU'(J)\mathbf{g} + \mu \operatorname{dev}[\bar{\mathbf{b}} - \tau^p], \quad \text{where} \quad \tau^p := \bar{\mathbf{F}}\mathbf{S}^p\bar{\mathbf{F}}^T \tag{3.3}$$

where $\bar{\mathbf{b}} := \bar{\mathbf{F}}\bar{\mathbf{F}}^T$. This stress strain relations derives from the stored energy $\Psi^o(\mathbf{E}) = 1/2\,\mu\,(I_{\bar{\mathbf{C}}} - 3) + U^o(J)$, where $I_{\bar{\mathbf{C}}} = \operatorname{tr}[\bar{\mathbf{C}}]$ is the first invariant of $\bar{\mathbf{C}}$ and $\mu > 0$ is a constant (shear modulus). The spatial elasticities are given by the expression

$$\begin{aligned} \mathbf{a}^0 &:= J^2U^{0\prime\prime}(J)\mathbf{g}\otimes\mathbf{g} + Jp(\mathbf{g}\otimes\mathbf{g} - 2\mathbf{I}) + \mathbf{a}^0_{\text{dev}} \\ \mathbf{a}^0_{\text{dev}} &:= \frac{2}{3}\mu I_{\bar{b}}[\mathbf{I} - \frac{1}{3}\mathbf{g}\otimes\mathbf{g}] - \frac{2}{3}\mu[\operatorname{dev}\mathbf{b}\otimes\mathbf{g} + \mathbf{g}\otimes\operatorname{dev}\bar{\mathbf{b}}] \end{aligned} \tag{3.4}$$

The elastic constitutive equation furnishes an uncoupled extension to the compressible range of the clasical neo-Hookean model.

3.2 Yield condition and flow rule. Hardening laws

Ignoring for the moment hardening effects, we assume the classical von Mises yield condition given by

$$\phi(\tau, \mathbf{g}) := \|\operatorname{dev}\tau\| - R := \sqrt{\tau^{ij}\tau^{kl}g_{ik}g_{jl} - \frac{1}{3}(\tau^{kl}g_{kl})^2} - R \tag{3.5a}$$

where R is the radius of the Mises sphere. Equivalently, employing $\mathbf{C} = 2\mathbf{E} + \mathbf{1}$ instead of $\mathbf{E}$ as basic strain variable, (3.5a) may be rephrased in the material setting as

$$\bar{\Phi}(\mathbf{C}, \mathbf{S}^p) := \phi(\mathbf{S}, \mathbf{C}) := \|\operatorname{DEV}\mathbf{S}\| - R := \sqrt{S^{IJ}S^{KL}C_{IK}C_{JL} - \frac{1}{3}(S^{KL}C_{KL})^2} - R \tag{3.5b}$$

where $\mathbf{S}^0 := 2\varrho_{\text{ref}}\partial\Psi^0(\mathbf{C})/\partial\mathbf{C}$ is a function of $\mathbf{C}$. Making use of the chain rule, the associativ flow rule (2.19) becomes

$$\dot{\mathbf{S}}^p = 2\dot{\gamma}\frac{\partial\bar{\Phi}(\mathbf{C}, \mathbf{S}^p)}{\partial\mathbf{C}} = 2\dot{\gamma}\left[\mathbf{A}^0 : \frac{\partial\phi(\mathbf{S}, \mathbf{C})}{\partial\mathbf{S}} + \frac{\partial\phi(\mathbf{S}, \mathbf{C})}{\partial\mathbf{C}}\right] \tag{3.6a}$$

where $\mathbf{A}^0 := 4\partial^2\Psi^0(\mathbf{C})/\partial\mathbf{C}^2$ are the material (initial) elasticities. We recall the following component relation between material and spatial elasticities $\mathbf{a}^0$,

$$a^{0ijkl} = 2F_I^i F_J^j F_K^k F_L^l A^{0IJKL}, \quad \text{where} \quad A^{0IJKL} = 4\frac{\partial^2\Psi}{\partial C_{IJ}\partial C_{KL}} \tag{3.6b}$$

Using this relation along with the fact that $L_v\tau^p = \mathbf{F}\dot{\mathbf{S}}^p\mathbf{F}^T$ [see Eq. 2.24)], (3.6a) may be rephrased in the spatial description in the following equivalent form

$$L_v\tau^p = \dot{\gamma}\left[\mathbf{a}^0 : \frac{\partial\phi(\tau,\mathbf{g})}{\partial\tau} + 2\frac{\partial\phi(\tau,\mathbf{g})}{\partial\mathbf{g}}\right] \tag{3.6c}$$

For the Mises yield criterion we have the expressions

$$\frac{\partial\phi(\tau,\mathbf{g})}{\partial\tau} := \mathbf{n} := \frac{\operatorname{dev}\tau}{\|\operatorname{dev}\tau\|}, \quad \text{and} \quad \frac{\partial\phi(\tau,\mathbf{g})}{\partial\mathbf{g}} = \|\operatorname{dev}\tau\|\mathbf{n}^2 \tag{3.7}$$

Since only $[\operatorname{dev}\tau]$ enters in the yield condition, $\mathbf{a}^0$ must be replaced by $\mathbf{a}^0_{\text{dev}}$. The latter is related to $\mathbf{A}^0_{\text{dev}} := 2\partial(\operatorname{DEV}\mathbf{S})/\partial\mathbf{C}$ by the push-forward relation (3.6b). Therefore, substitutions of (3.7) into (3.6c) yields the following associative flow rule

$$L_v\tau^p = \dot{\gamma}[\mathbf{a}^0_{\text{dev}} : \mathbf{n} + 2R\mathbf{n}^2] \approx \dot{\gamma}\,\mathbf{a}^0_{\text{dev}} : \mathbf{n} \tag{3.8}$$

We note that the ratio of the second over the first term in (3.8) is of the order of the flow stress over the modulus; i.e, R/μ. Hence, for most metals the second term is negligible. Although not essential, we shall assume this is the case in what follows.

In view of expression (3.8), it would appear that the full Lie derivative $L_v\tau^p$ enters in the formulation of the rule. However, it can be shown that actually only the deviatoric part of $L_v\tau^p$ is relevant; i.e., the part

$$\operatorname{dev} L_v\tau^p = 2\bar{\mu}\dot{\gamma}\mathbf{n} \tag{3.9a}$$

where $\bar{\mu} := J^{-2/3}\operatorname{tr}\bar{\mathbf{b}}\mu/3$. Note that (3.9a) is analogous to the classical Levi-Saint Venant flow rule. Finally, in keeping with the assumption that volumetric response is uncoupled from plastic flow, we introduce the additional assumption that

$$\operatorname{tr}\tau^0 = 0 \quad \Rightarrow \operatorname{dev}\tau^p = \tau^p \tag{3.9b}$$

3.2.1 Kinematic/isotropic hardening

The proposed extension to the finite strain range of the classical Prager-Ziegler line kinematic hardening law is based on the following simple observation. In the infinitesimal case, classical J_2-flow theory may be formulated as

$$\begin{aligned} \mathbf{s} &= \mathbf{s} - \mathbf{s}^p & \boldsymbol{\alpha} &= \frac{h'}{3\mu}\mathbf{s}^p \\ \dot{\mathbf{s}}^p &= 2\bar{\mu}\dot{\gamma}\mathbf{n} & \bar{e}^p &= \dot{\gamma}\sqrt{\frac{2}{3}} \end{aligned} \tag{3.10}$$

That is, the back stress $\boldsymbol{\alpha}$ is proportional to the plastic stress $\mathbf{s}^p := 2\mu\boldsymbol{\varepsilon}^p$ with proportionality constant the non-dimensional factor $[h'/3\mu]$. We propose to retain exactly the same structure in the finite strain case. This leads to a set of constitutive equations which, for convencience, have been summarized in Box 3.

Remark 3.1. As already pointed out, in the presence of damage degradation the elastoplastic constitutive equations summarized in Box 3 remain unchanged provided that the stresses are replaced by effective stresses. This leads to a very simple algorithmic framework as discussed in Sect. 4.2. □

Box 3. Strain space J_2-flow theory at finite strain

(i) Additive stress split with uncoupled pressure:

$$\mathbf{s}^o := J^{-2/3}\mu\,\mathrm{dev}\,\mathbf{b}; \qquad \mathbf{s}^p := J^{-2/3}\,\mathrm{dev}\,\boldsymbol{\tau}^p$$

$$\boldsymbol{\tau} = K\ln J\mathbf{g} + \mathbf{s}^o - \mathbf{s}^p$$

(ii) Hardening law:

$$\beta\in[0,1], \varkappa_0 > 0, \text{ and } \bar{\mu} := \frac{\mu}{3} J^{-4/3}\,\mathrm{tr}\,\mathbf{b}$$

$$\varkappa(\bar{e}^p) = \varkappa_0 + \beta h' \bar{e}^p$$

$$\boldsymbol{\alpha}: = \frac{h'}{3\mu}(1-\beta)\mathbf{s}^p$$

$$\dot{\bar{e}}^p = \sqrt{\frac{2}{3}}\dot{\gamma}$$

(iii) Yield condition

$$(\boldsymbol{\xi} := \mathrm{dev}\,\boldsymbol{\tau} - \boldsymbol{\alpha})$$

$$\Phi := \|\boldsymbol{\xi}\| - \sqrt{\frac{2}{3}}\varkappa(\bar{e}^p) \le 0$$

(iv) Plastic flow rule:

$$\mathrm{dev}\,L_v\boldsymbol{\tau}^p = 2\bar{\mu}\dot{\gamma}\mathbf{n}, \qquad \mathrm{tr}\,\boldsymbol{\tau}^p = 0$$

$$\text{where } \mathbf{n} := \frac{\boldsymbol{\xi}}{\|\boldsymbol{\xi}\|}$$

4 Algorithmic treatment

In this section, we consider the algorithmic treatment of the proposed damage-elastoplaticity formulation. Concerning the damage part, the strain-based nature of the proposed damage mechanism results in a trivial integration procedure for the damage variable. Its discussion is thus postponed to Sect. 4.2 where the general case is considered.

As a motivation for the integration algorithm proposed for the elastoplastic part, we first examine in detail the hyperplastic extension of the J_2-flow theory outlined in the previous section. It is shown that incrementally objective algorithms to integrate hypoelastic constitutive equations are no longer necessary. Evaluation of the elastic predictor reduces to a mere function evaluation. In addition, the consistent integrator for the flow rule reduces to the classical radial return of Wilkins (1964), and Krieg and Krieg (1977). Thus, from a computational standpoint, the only difference with the infinitesimal case is that finite strain kinematics is employed in the evaluation of the elastic predictor. The plastic corrector (return mapping) phase is exactly the same as in the infinitesimal case.

4.1 Plastic response. Extension of Wilkin's radial return algorithm

We recall that from a computational point of view the basic problem may always be regarded as strain driven. Accordingly, assume that at time t_n the configuration $\boldsymbol{\phi}_n(\mathbf{X})$ and the plastic variables $\{\boldsymbol{\tau}_n^p, \bar{e}_n^p\}$ are known. The problem is to update the basic variables $\{\boldsymbol{\tau}_n^p, \bar{e}_n^p\}$ for a given incremental displacement $\mathbf{u}: \boldsymbol{\phi}_n(\Omega) \to \mathbb{R}^3$.

4.1.1 Configuration update. Elastic predictor

Since the update process is strain driven for a given incremental displacement $\mathbf{u}(\mathbf{x}_n)$, where $\mathbf{x}_n = \boldsymbol{\phi}_n(\mathbf{X})$, the configuration is trivially updated (exactly) by the kinematic relations collected in step (i) of Box 1. There, we have set $\mathbf{U}(\mathbf{X}) := \mathbf{u}(\boldsymbol{\phi}_n(\mathbf{X}))$, where $\mathbf{X}$ designates the position of a particle in the reference configuration which at t_n occupies $\mathbf{x}_n := \boldsymbol{\phi}_n(\mathbf{X})$.

Thus, the initial elastic (predictor) stress deviator is computed by function evaluation as

$$\operatorname{dev}[\boldsymbol{\tau}^0_{n+1}] = \mu \operatorname{dev}[\bar{\mathbf{F}}\,\bar{\mathbf{F}}^T] \tag{4.1}$$

The final stress is then computed simply as $\boldsymbol{\tau}_{n+1} = \boldsymbol{\tau}^0_{n+1} - \boldsymbol{\tau}^p_{n+1}$, once the platic strain $\boldsymbol{\tau}^p_{n+1}$ is obtained. Damage degradation is trivially accommodated in the elastic-damage predictor due to the strain-diven nature of the proposed damage model. The appropriate generalization is contained in steps (i)–(iii) of Box 6.

4.1.2 Integration of the plastic flow rule

As in the infinitesimal theory, an implicit backward-Euler difference scheme is employed to integrate the plastic flow rule. In the material setting we have

$$\mathbf{S}^p_{n+1} = \mathbf{S}^p_n + \gamma_{n+1}\mathbf{A}^0_{n+1} : \mathbf{N}_{n+1} \tag{4.2}$$

where $\mathbf{N}_{n+1} := [\operatorname{DEV}\mathbf{S}_{n+1} - \boldsymbol{\Gamma}_{n+1}]/\|\operatorname{DEV}\mathbf{S}_{n+1} - \boldsymbol{\Gamma}_{n+1}\|$, and $\boldsymbol{\Gamma}_{n+1} := \mathbf{F}^{-1}_{n+1}\,\boldsymbol{\alpha}_{n+1}\mathbf{F}^{-T}_{n+1}$ is the pull-back of the spatial back stress $\boldsymbol{\alpha}_{n+1}$. By transforming (4.2) to the current configuration (push-forward) we obtain

$$\begin{aligned} &\boldsymbol{\tau}^p_{n+1} = \mathbf{F}_{\mathbf{u}}\boldsymbol{\tau}^p_n\mathbf{F}^T_{\mathbf{u}} + \gamma_{n+1}\,\mathbf{a}^0_{\operatorname{dev}n+1} : \mathbf{n}_{n+1} \\ &\mathbf{F}_{\mathbf{u}} := \mathbf{F}_{n+1}\mathbf{F}^{-1}_n, \qquad \mathbf{n}_{n+1} := \frac{\boldsymbol{\tau}_{n+1} - \boldsymbol{\alpha}_{n+1}}{\|\boldsymbol{\tau}_{n+1} - \boldsymbol{\alpha}_{n+1}\|} \end{aligned} \tag{4.3}$$

Next, we compute $\mathbf{s}^p_{n+1}$ as follows. Noting that

$$J^{-2/3}\operatorname{dev}[\mathbf{a}^0_{\operatorname{dev}n+1} : \mathbf{n}_{n+1}] := 2\bar{\mu}\,\mathbf{n}_{n+1}, \quad \text{where} \quad \bar{\mu} := J^{-2/3}\frac{1}{3}I_{\mathbf{b}}\mu \tag{4.4}$$

we obtain the expression

$$\mathbf{s}^p_{n+1} := J^{-2/3}_{n+1}\operatorname{dev}\boldsymbol{\tau}^p_{n+1} = J^{-2/3}_{n+1}\operatorname{dev}[\mathbf{F}_{\mathbf{u}}\boldsymbol{\tau}^p_n\mathbf{F}^T_{\mathbf{u}}] + 2\bar{\mu}\gamma_{n+1}\mathbf{n}_{n+1} \tag{4.5}$$

However, since $\det\mathbf{F}_{\mathbf{u}} = J_{n+1}/J_n$ and, by assumption, $\operatorname{dev}\boldsymbol{\tau}_n = \boldsymbol{\tau}_n$, setting $\bar{\mathbf{F}}_{\mathbf{u}} := (\det\mathbf{F}_{\mathbf{u}})^{-1/3}\mathbf{F}_{\mathbf{u}}$ leads to

$$\mathbf{s}^{p\,\text{trial}}_{n+1} = \operatorname{dev}[\bar{\mathbf{F}}_{\mathbf{u}}(J^{-2/3}_n\operatorname{dev}\boldsymbol{\tau}^p_n)\bar{\mathbf{F}}^T_{\mathbf{u}}] := \operatorname{dev}[\bar{\mathbf{F}}_{\mathbf{u}}\mathbf{s}^p_n\bar{\mathbf{F}}^T_{\mathbf{u}}] \tag{4.6}$$

Thus, on account of the rate free definition $\boldsymbol{\alpha}_{n+1} = h'/3\mu\,(1-\beta)\,\mathbf{s}^p_{n+1}$ for the back stress, we arrive at the following update formulae

$$\begin{aligned} &\mathbf{s}^{p\,\text{trial}}_{n+1} := \operatorname{dev}[\bar{\mathbf{F}}_{\mathbf{u}}\mathbf{s}^p_n\bar{\mathbf{F}}^T_{\mathbf{u}}], \qquad \mathbf{s}^{\text{trial}}_{n+1} := \mu\operatorname{dev}[\bar{\mathbf{F}}_{n+1}\bar{\mathbf{F}}^T_{n+1}] - \mathbf{s}^{p\,\text{trial}}_{n+1} \\ &\boldsymbol{\xi}^{\text{trial}}_{n+1} := \mathbf{s}^{\text{trial}}_{n+1} - \frac{h'}{3\mu}(1-\beta)\,\mathbf{s}^{p\,\text{trial}}_{n+1}, \qquad \boldsymbol{\xi}_{n+1} = \boldsymbol{\xi}^{\text{trial}}_{n+1} - 2\bar{\mu}\gamma_{n+1}\left[1 + (1-\beta)\frac{h'}{3\mu}\right]\mathbf{n}_{n+1} \end{aligned} \tag{4.7}$$

Finally, from $(4.7)_4$ we observe that $\mathbf{n}_{n+1}$ and the plastic consistency parameter can be computed in closed form exclusively from the predictor (trial) values according to the expressions

$$\mathbf{n}_{n+1} = \frac{\boldsymbol{\xi}^{\text{trial}}_{n+1}}{\|\boldsymbol{\xi}^{\text{trial}}_{n+1}\|}, \qquad 2\bar{\mu}\gamma_{n+1} = \frac{\|\boldsymbol{\xi}^{\text{trial}}_{n+1}\| - R_n}{1 + \dfrac{h'}{3\mu}(1-\beta) + \dfrac{\beta h'}{3\bar{\mu}}} \tag{4.8}$$

Note that the equivalent plastic strain is trivially updated by the backward-Euler formula $\bar{e}^p_{n+1} = \bar{e}^p_n + \sqrt{2/3}\,\gamma_{n+1}$ once the consistency parameter γ_{n+1} is found. A step-by-step summary of the algorithm is contained in Box 4. Note that, except for the push-forward of the plastic stress $\boldsymbol{\tau}^p_n$, the algorithm of the infinitesimal theory remains unchanged.

Box 4. Hyperelastic extension of the radial return algorithm

(i) Geometric update and volume preserving tensors:

$$\boldsymbol{\phi}_{n+1} = \boldsymbol{\phi}_n + \mathbf{U}; \quad \mathbf{F}_{n+1} := \mathbf{F}_n + \mathrm{GRAD}\,\mathbf{U}$$

$$J_{n+1} = \det \mathbf{F}_{n+1}; \quad \bar{\mathbf{b}}_{n+1} := J_{n+1}^{-2/3}\,\mathbf{F}_{n+1}\,\mathbf{F}^T_{n+1}$$

$$\mathbf{F}_{\mathbf{u}} = \mathbf{F}_{n+1}\mathbf{F}_n^{-1}; \quad \bar{\mathbf{F}}_{\mathbf{u}} := (\det \mathbf{F}_{\mathbf{u}})^{-1/3}\,\mathbf{F}_{\mathbf{u}}$$

(ii) Elastic predictor: (hyperelastic potential and stress split)

$$\mathbf{s}^{p\,\mathrm{trial}}_{n+1} = \mathrm{dev}\,[\bar{\mathbf{F}}_{\mathbf{u}}\,\mathbf{s}^p_n\,\bar{\mathbf{F}}^T_{\mathbf{u}}]$$

$$\mathbf{s}^{\mathrm{trial}}_{n+1} = \mu\,\mathrm{dev}\,\bar{\mathbf{b}}_{n+1} - \mathbf{s}^{p\,\mathrm{trial}}_{n+1}$$

$$\boldsymbol{\xi}^{\mathrm{trial}}_{n+1} = \mathbf{s}^{\mathrm{trial}}_{n+1} - \frac{h'}{3\mu}(1-\beta)\,\mathbf{s}^{p\,\mathrm{trial}}_{n+1}$$

(iii) Check for yielding:

$$\text{IF } \phi^{\mathrm{trial}}_{n+1} := \|\boldsymbol{\xi}^{\mathrm{trial}}_{n+1}\| - \sqrt{\frac{2}{3}}\,\boldsymbol{\varkappa}(\bar{e}^p_n) \le 0 \text{ THEN}$$

Set $(\cdot)_{n+1} = (\cdot)^{\mathrm{trial}}_{n+1}$ and EXIT

ELSE

(iv) Radial return scheme:

$$\mathbf{n}_{n+1} = \frac{\boldsymbol{\xi}^{\mathrm{trial}}_{n+1}}{\|\boldsymbol{\xi}^{\mathrm{trial}}_{n+1}\|}, \qquad 2\bar{\mu}\gamma_{n+1} = \frac{\phi^{\mathrm{trial}}_{n+1}}{1 + \dfrac{h'}{3\mu}(1-\beta) + \dfrac{\beta h'}{3\bar{\mu}}}$$

$$\bar{e}^p_{n+1} = \bar{e}^p_n + \sqrt{\frac{2}{3}}\,\gamma_{n+1}$$

$$\mathbf{s}^p_{n+1} = \mathbf{s}^{p\,\mathrm{trial}}_{n+1} + 2\bar{\mu}\gamma_{n+1}\,\mathbf{n}_{n+1}$$

$$\mathbf{s}_{n+1} = \mathbf{s}^{\mathrm{trial}}_{n+1} - 2\bar{\mu}\gamma_{n+1}\,\mathbf{n}_{n+1}$$

(v) Compute consistent tangent modulus:

See Box 5 □

Remark 4.1. The case in which the isotropic and kinematic hardening moduli are nonlinear functions of the equivalent plastic strain $\bar{e}^p$ can be readily incorporated into the algorithm in Box 4 exactly as in Simo and Taylor (1985). We recall that one only needs to solve a scalar equation by a Newton iteration. □

Remarkably, the algorithm summarized in Box 4 can be linearized exactly leading to a closed form expression for the so-called consistent elastoplastic tangent modulus. We refer to the Appendix for details. The final result for the isotropic case is contained in Box 5. Use of the consistent modulus

(and not the continuum modulus in Box 1) is essential in preserving the asymptotic rate of quadratic convergence in the Newton's method (Simo and Taylor 1985). The resulting modulus is non-symmetric due to the integration algorithm. However, numerical experiments indicate that symmetrization does not result in loss of quadratic rate of convergence.

Box 5. Consistent (symmetrized) deviatoric elastoplastic tangent modulus

(i) Moduli associated with the *trial deviatoric* stress state:

$$I_{n+1}^{\text{trial}} := \mu \operatorname{tr} \bar{\mathbf{b}}_{n+1} - \operatorname{tr}[\bar{\mathbf{F}}_{\mathbf{u}}\, \mathbf{s}_n^p\, \bar{F}_u]$$

$$\mathrm{a}_{\mathrm{dev}\,n+1}^{\text{trial}} := \frac{2}{3} I_{n+1}^{\text{trial}} \left[\boldsymbol{I} - \frac{1}{3} \mathbf{g} \otimes \mathbf{g} \right] - \frac{2}{3} [\mathrm{s}_{n+1}^{\text{trial}} \otimes \mathbf{g} + \mathbf{g} \otimes \mathrm{s}_{n+1}^{\text{trial}}]$$

(ii) Scaling factors

$$f_0 := 1 - \frac{2\bar{\mu}\gamma_{n+1}}{\|s_{n+1}^{\text{trial}}\|} \qquad \delta_0 = 1 + \frac{h'}{3\bar{\mu}} \qquad f_1 := \left[\frac{1}{\delta_0} - 1 + f_0 \right]$$

$$\delta_1 := f_1 \frac{2}{3} I_{n+1}^{\text{trial}} \qquad \delta_2 := \left[\frac{1}{\delta_0} - 1 \right] \frac{4}{3} \bar{\mu}\gamma_{n+1} - \frac{2}{3} \|\mathbf{s}_{n+1}^{\text{trial}}\| f_1$$

$$\delta_3 := 2\|\mathbf{s}_{n+1}^{\text{trial}}\| f_1 \qquad \delta_4 := \left[\frac{1}{\delta_0} - 1 \right] \frac{4}{3} \mu\gamma_{n+1} J^{-2/3}$$

(iii) Consistent (symmetrized) tangent modulus:

$$\mathbf{a}_{\mathrm{dev}\,n+1}^{ep} := f_0\, \mathbf{a}_{n+1}^{\text{trial}} - \delta_1 \mathbf{n} \otimes \mathbf{n} - \delta_2 [\mathbf{n} \otimes \mathbf{g}]^s - \delta_3 [\mathbf{n} \otimes \mathbf{n}^2]^s + \delta_4 [\mathbf{n} \otimes \operatorname{dev} \bar{\mathbf{b}}_{n+1}]^s$$

4.2 General elastic-damage-plastic return mapping algorithm

The algorithmic ideas discussed above can be readily extended to the general situation summarized in Boxes 1 and 2. The corner stone in the treatment of the plastic response is the cutting plane algorithm proposed in Simo and Ortiz (1985), and further analyzed in Ortiz and Simo (1986), suitably modify to accommodate the present formulation. The detail have been summarized in Box 6. Note that strain-based damage models of the type in Box 2 are trivially incorporated in the present algorithmic framework through step (ii).

Box 6. Stress update algorithm. Spatial setting

(i) Geometric update:

$$\boldsymbol{\phi}_{n+1} = \boldsymbol{\phi}_n + \mathbf{u}(\mathbf{x}_n); \qquad \mathbf{F}_{\mathbf{u}} = \mathbf{1} + \nabla_{\mathbf{x}_n} \mathbf{u}(\mathbf{x}_n)$$

$$\mathbf{F}_{n+1} = \mathbf{F}_{\mathbf{u}} \mathbf{F}_n; \qquad \mathbf{C}_{n+1} = \mathbf{F}_{n+1}^T \mathbf{F}_{n+1}$$

(ii) Damage evolution:

$$\bar{\tau}_{n+1} := \sqrt{2\Psi^o(\mathbf{C}_{n+1})} \quad \text{and} \quad r_{n+1} := \max\{r_n, \bar{\tau}_{n+1}\}.$$

$$d_{n+1} = \begin{cases} d_n & \text{if } \bar{\tau}_{n+1} - r_n \le 0 \\ G(\bar{\tau}_{n+1}) & \text{otherwise} \end{cases}$$

(iii) Elastic-damage predictor: By using hyperelastic potential and stress split:

$\bar{\tau}_{n+1}^{p(\text{trial})} = \mathbf{F}_{\mathbf{u}}\, \bar{\tau}_n^p\, \mathbf{F}_{\mathbf{u}}^T, \quad \mathbf{q}_{n+1}^{\text{trial}} = \text{push-forward of } \mathbf{q}_n \text{ by } \mathbf{F}_{\mathbf{u}}$

$$\bar{\tau}_{n+1}^{o} = 2\varrho_{\text{ref}} \frac{\partial \Psi^o(\mathbf{g}, \mathbf{F}_{n+1})}{\partial \mathbf{g}}, \quad \bar{\tau}_{n+1}^{\text{trial}} = \bar{\tau}_{n+1}^{o} - \bar{\tau}_{n+1}^{p(\text{trial})}$$

(iv) Check for yielding:

$\phi_{n+1}^{\text{trial}} := \phi(\bar{\tau}_{n+1}^{\text{trial}}, \mathbf{g}, \mathbf{q}_{n+1}^{\text{trial}})$

IF $\phi_{n+1}^{\text{trial}} \leq 0$ THEN: Set $(.)_{n+1} = (.)_{n+1}^{\text{trial}}$ and EXIT.

ELSE: Set $i = 0$ and GO TO (v)

(v) Plastic corrector:

$$\text{Set } \Sigma_{n+1}^{(i)} := \left[\frac{\partial \phi}{\partial \bar{\tau}} : \mathbf{a}^o : \frac{\partial \phi}{\partial \bar{\tau}} + 2 \frac{\partial \phi}{\partial \mathbf{g}} : \frac{\partial \phi}{\partial \bar{\tau}} - \frac{\partial \phi}{\partial \mathbf{q}} \cdot \mathbf{h} \right]_{n+1}^{(i)}$$

$$\Delta\gamma_{n+1}^{(i+1)} = \phi_{n+1}^{(i)} / \Sigma_{n+1}^{(i)}$$

$$\bar{\tau}_{n+1}^{p(i+1)} = \bar{\tau}_{n+1}^{p(i)} + \Delta\gamma_{n+1}^{(i+1)} \left[\mathbf{a}^o : \frac{\partial g}{\partial \bar{\tau}} + 2 \frac{\partial g}{\partial \mathbf{g}} \right]_{n+1}^{(i)}$$

$$\bar{\tau}_{n+1}^{(i+1)} = \bar{\tau}_{n+1}^{(i)} - \Delta\bar{\tau}_{n+1}^{p(i+1)}; \quad \mathbf{q}_{n+1}^{(i+1)} = \mathbf{q}_{n+1}^{(i)} + \Delta\gamma_{n+1}^{(i+1)}\, \mathbf{h}_{n+1}^{(i)}$$

(vi) Check for convergence:

$\phi_{n+1}^{(i+1)} := \phi(\bar{\tau}_{n+1}^{(i+1)}, \mathbf{g}, \mathbf{q}_{n+1}^{(i+1)})$

IF $\phi_{n+1}^{(i+1)} < \text{TOL}$ THEN: Set $(.)_{n+1} = (.)_{n+1}^{(i+1)}$ and EXIT.

ELSE: Set $i \leftarrow i + 1$ and GO TO (v).

Remark 4.2. (Viscous damage case). The algorithm summarized in Box 6 can be readily extended to accommodate the rate-dependent viscous-damage model outlined in Remark 4.3. The basic idea is to consider a generalized mid-point rule algorithm for the intergration of the evolution equations in Box 1.a. Standard results (i.e., Hughes 1987) show that the algorithm is unconditionally stable for $\alpha \geq 1/2$ and second order accurate for $\alpha = 1/2$. The details involved in the calculation, which replaces steps (i) and (ii) in Box 6, have been summarized for convenience in Box 7. □

Box 7. Viscous-damage algorithm at finite strains

1. Geometric update:

$\boldsymbol{\phi}_{n+1} = \boldsymbol{\phi}_n + \mathbf{u}(\mathbf{x}_n); \quad \mathbf{F}_{\mathbf{u}} = \mathbf{1} + \nabla_{\mathbf{x}^n} \mathbf{u}$

$\mathbf{F}_{n+1} = \mathbf{F}_{\mathbf{u}}\, \mathbf{F}_n; \quad \mathbf{C}_{n+1} = \mathbf{F}_{n+1}^T\, \mathbf{F}_{n+1}$

2. Viscous damage evolution of damage:

$\mathbf{F}_{n+\alpha} = \alpha \mathbf{F}_{n+1} + (1-\alpha)\, \mathbf{F}_n, \quad \mathbf{C}_{n+\alpha} := \mathbf{F}_{n+\alpha}^T\, \mathbf{F}_{n+\alpha} \quad \bar{\tau}_{n+\alpha} := \sqrt{2\, \Psi^o(\mathbf{C}_{n+\alpha})}$

2.1 Check for damage loading:

$g_{n+\alpha}^{\text{trial}} := \bar{\tau}_{n+\alpha} - r_n$

IF $g_{n+1}^{\text{trial}} \leq 0$ THEN:

$r_{n+1} = r_n$

$d_{n+1} = d_n$

ELSE:

$$r_{n+1} = \frac{r_n + \Delta t/\eta\, \bar{\tau}_{n+\alpha}}{1 + \alpha \Delta t/\eta}$$

$$d_{n+1} = d_n + \frac{\Delta t}{1 + \alpha \Delta t/\eta} [\tau_{n+\alpha} - r_n] G'(\bar{\tau}_{n+\alpha})$$

END IF

5 Numerical simulations

In this section, the performance of proposed elastic-damage, elastoplastic, and elastoplastic-damage constitutive models summarized in Boxes 1–3 is illustrated through nine numerical simulations. Our finite element treatment relies on a mixed variational formulation of the Hu-Washizu type, as described in Simo et al. (1985), and Simo (1986). The numerical implementation is done in an extended version of the general purpose Finite Element Analysis Program (FEAP), developed by R.L. Taylor and documented in Chapt. 24 in Zienkiewicz (1977), and employs the four-node element with bi-linear isoparametric displacement field and constant (current) volume. All the calculations were performed in a CONVEX C-1 mini-supercomputer under UNIX 4.2 BSD operating system at Stanford University, and a VAX 780 under Berkeley-UNIX 4.3 BSD operating system at the University of California, Berkeley.

5.1 Numerical solution strategies

A combination of BFGS updates and line search with periodic re-factorizations in the initial stages, followed by a standard Newton iteration once the residual norm is suitably reduced, proved to be the most effective solution technique for the proposed formulation. The use of an inaccurate linear line search algorithm proves to be essential for a robust numerical performance. Our computational experience also indicates that a fixed number of BFGS updates prior to a new re-factorization, as in Matthies and Strang (1979), Bathe and Cimento (1980), Bathe and Sonnad (1980) or Hallquist (1983), is not necessarily optimal. Convergence is assumed to take place when the energy norm of the iterate is 10^{-18} times the maximum value attained by the energy norm in the current time step.

Isotropic hardening is characterized by means of the following hardening law of the saturation type

$$\varkappa(\bar{e}^p) := Y_\infty - (Y_\infty - Y_0) e^{-\delta \bar{e}^p} + \zeta \bar{e}^p, \qquad \delta > 0, \zeta \geq 0. \tag{5.1}$$

5.2 Quasi-static damage propagation of notched specimens

We consider quasi-static damage propagation (microcrack and macrocrack growth) in notched specimens under tension and plane strain condition for both the elastic-damage and elastoplastic-damage models. Of particular interest is the coupling between the plasticity and damage mechanisms. It is shown that due to the strain-based characterization of damage, the model predicts higher damage accumulation in the specimens considered in the presence of plastic flow. This is in agreement with experimental observations and the so-called "plastic correction" procedure typically employed in the fracture mechanics (e.g., Knott 1973; Atluri et al. 1984, 1985).

Two finite element meshes are utilized in these "Mode I" fracture simulations, consisting of 288 elements and 1152 elements, respectively, as shown in Figs. 1 and 2. This sub-division of the finite element mesh was considered to assess mesh-dependency due to a possible strain-softening response; (e.g., Willam 1987; Bazant and Belytschko 1987. The calculations are performed with the following damage accumulation function (Mazars 1982)

$$d := G(\bar{\tau}) = 1 - \frac{\bar{\tau}_0(1-A)}{\tau} - A\exp\left[B(\bar{\tau}_0 - \bar{\tau})\right] \tag{5.2}$$

Here A and B are characteristic material parameters and $\bar{\tau}_0$ denotes the initial damage threshold. The numerical values of the material properties used in computation are taken to be $E = 206.916$ GPa, $v = 0.29$, $A = 0.85$, $B = 2$, and $\bar{\tau}_0 = 0.02$ (GPa)$^{1/2}$. The numerical values of the constants in hardening law (5.1) are $Y_0 = 0.45$ GPa, $Y_\infty = 0.715$ GPa, $\delta = 16.93$, and $\zeta = 20$ GPa.

The specimens are under displacement boundary control. As the magnitude of the control displacement is increased, one observes a corresponding increase in value of the damage parameter d in the elements ahead of the tip of the notch. Eventually, complete damage (corresponding to $d = 0.99$) is obtained. Thus, crack propagation is characterized as the locus of points for which the damage parameter d attains the value $d = 0.99$. Figure 3 shows the load-deflection curves of the entire loading histories for the 288 and 1152-element meshes. From this Figure one notes that the mesh sensitivity is not too significant. For instance, changes in the peak response do not surpass 11%–14%. We also observe that the number of fully damaged elements increases as the crack mouth opening displacement (CMOD) is increased. For clarity, the number of fully damaged ("cracked") elements versus the time steps for the elastic-damage case is summarized for both meshes in Table 1.

For the case of elastoplastic-damage, the relationship between the number of fully damaged elements, the number of yielded elements, and the time-step count is shown in Table 2 (for both

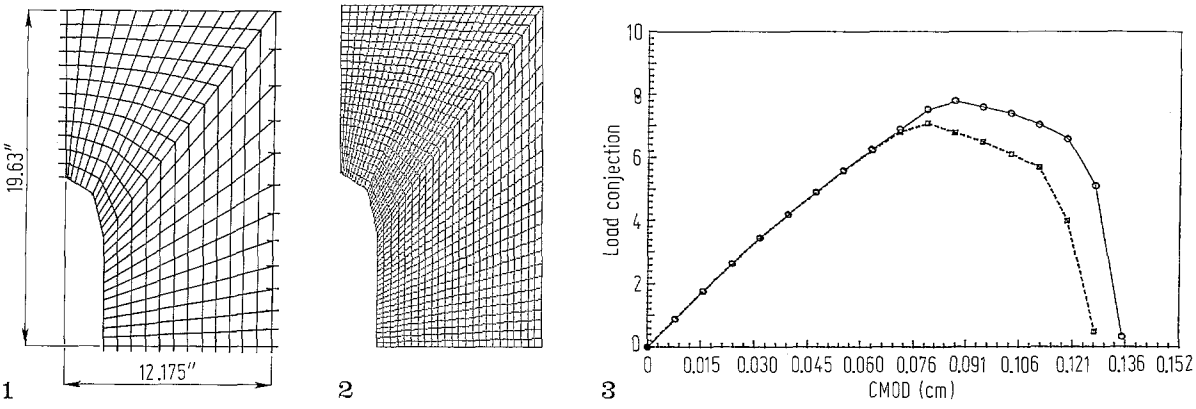

Figs. 1–3. 1, 2 Finite damage of a notched; finite element mesh (**1** 288 elements; **2** 1152 elements). **3** Finite elastic-damage of a notched specimen; the global load-deflection curves for 288 and 1152-element meshes

Table 1. No. "cracked" elmt. vs. time steps (Elastic-damage)

Step	No. (288-mesh)	No. (1152-mesh)
10	0	2
11	1	6
12	3	9
13	4	12
14	5	15
15	6	19
16	7	24
17	12	24

Table 2. No. "cracked" elmt. vs. time steps (El.-pl.-damage)

Step	No. crack (288)	No. yld. (288)	No. crack (1152)	No. yld. (1152)
5	0	1	2	9
6	1	6	8	18
7	4	7	11	19
8	5	9	14	21
9	6	10	18	23
10	7	11	19	24
11	8	12	21	24
12	9	12	23	24
13	10	12	24	24
14	12	12	24	24

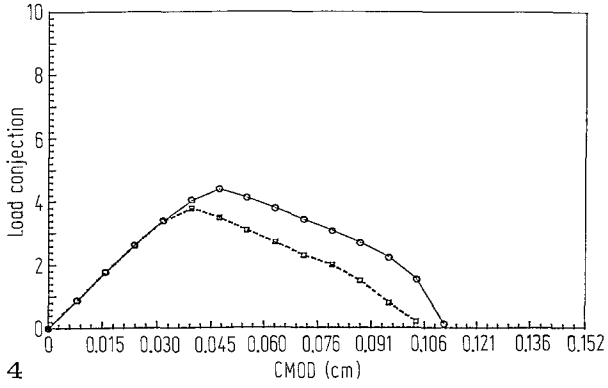

4

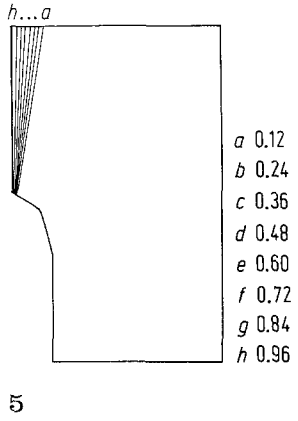

5

Figs. 4 and 5. 4 Finite elastoplastic-damage of a notched specimen; the global load-deflection curves for 288 and 1152-element meshes. **5** Finite damage of a notched specimen; the damage contours corresponding to a through crack

meshes). One should note that the number of yielded elments is always higher than that of fully damaged elements; and that the latter number increases with the former number. This illustrates the strong coupling between plasticity and damage exibited by the model, and demonstrates the fundamental role played by plastic flow in the growth of damage. Such a mode of response is in qualitative agreement with available physical evidence. Figure 4 shows the load-deflection curves of the entire loading histories for the 288 and 1152-element meshes. We emphasize once more that these fully damaged elements represent a physical macrocrack ahead of the original tip of the notch, with the damage contours shown in Fig. 5.

5.3 A set of test problems for finite strain elastoplasticity

We propose to asses the performance of the present elastoplastic formulation, which is based on an additive split of the stress tensor, on the basis of a complete set of problems that include simulations considered separately by several authors in the recent computational literature. This set of problems has been employed recently in Simo (1988 b, c) to asses the performance of a hyperelastic formulation of elastoplasticity based on the multiplicative decomposition.

5.3.1 Simple tension and simple shear

To ensure quasi-incompressible response the material properties are chosen to be

$$K = 4000 \text{ MPa}, \ \mu = 300 \text{ MPa}, \ Y_0 = Y_\infty = 0.5 \text{ MPa}, \ \zeta = 0 \text{ MPa} \tag{5.3}$$

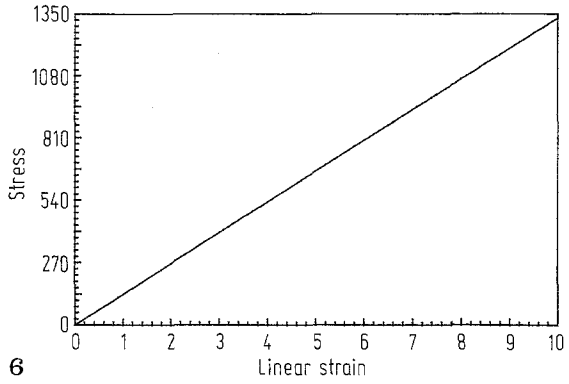

6

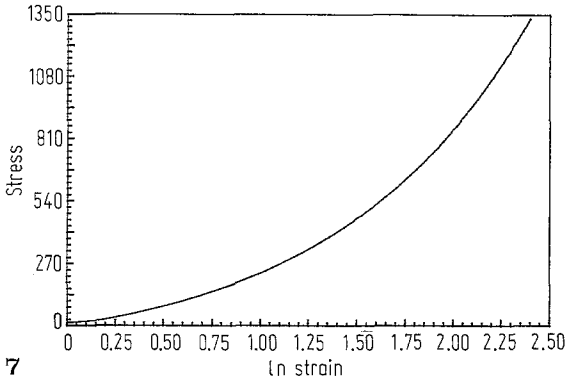

7

Figs. 6 and 7. The stress-strain curve for pure shear with pure kinematic hardening law; the strain is **6** in a linear scale, and **7** in a logarithmic scale

The numerical simulation reproduced the exact solutions for simple tension in the 2-direction ($\sigma_{22} = 0.5$ MPa, and all other components zero), and simple shear in the 1–2 plane (only one non-zero component $\sigma_{12} = 0.2887$ MPa).

Of particular interest is the response in a (homogeneous) pure shear deformation under a pure kinematic (linear) hardening law. As first noted by Nagtegaal and de Jong (1981 b) this example gives rise to a spurious oscillatory stress-strain response when the kinematic hardening law is described in terms of the Jaumann derivative. The computed results shown in Fig. 6 in a linear scale, and in Fig. 7 in a logarithmic scale, are obtained for the following values of the material parameters: $K = 40000$ MPa, $\mu = 3800$ MPa, $h' = 414$, and a radius of Mises yield surface of 0.40825 MPa. Figure 6 shows that the proposed rate-free extension of the Prager-Ziegler kinematic hardening law leads to a stress-strain curve which is not only monotonically increasing as in some rate formulations proposed in the past (e.g., Key 1984) but exactly linear. Note that the prsent formulation of the kinematic hardening law entirely bypasses the chase for the "proper" objective rate.

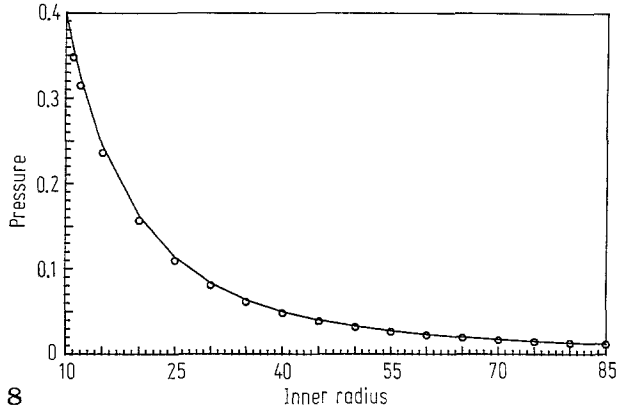

8

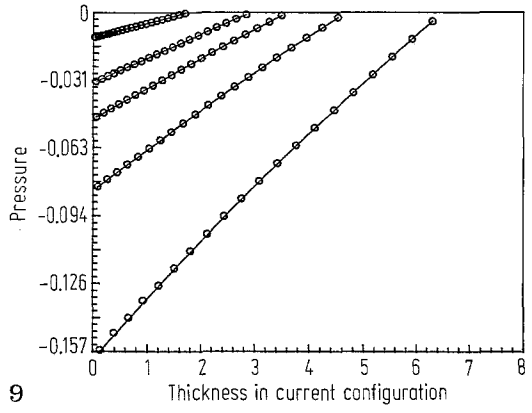

9

Figs. 8 and 9. A thick-wall cylinder under internal pressure; **8** pressure vs. the inner radius; **9** pressure profile at various configurations

Table 3. Number of iterations for each time step

Step	1	2	3	4	5
Count	6	6	6	6	6
Step	6	7	8	9	10
Count	6	5	5	5	5
Step	11	12	13	14	15
Count	5	5	5	5	5

Table 4. Energy norm values for some typical steps

Iteration	1	2	3	4	5	6
Step 1	0.220e + 8	0.244e + 5	0.103e + 3	0.516e − 2	0.235e − 10	0.382e − 23
Step 5	0.176e + 9	0.258e + 4	0.189e + 0	0.331e − 8	0.287e − 17	0.226e − 22
Step 9	0.488e + 9	0.457e + 3	0.703e − 2	0.298e − 10	0.735e − 19	...
Step 13	0.957e + 9	0.130e + 3	0.654e − 3	0.361e − 11	0.173e − 19	...
Step 15	0.125e + 10	0.780e + 2	0.247e − 4	0.168e − 11	0.109e − 19	...

Table 5. Residual norm values for some typical steps

Iteration	0	1	2	3	4	5
Step 1	0.326e + 7	0.332e + 5	0.421e + 4	0.494e + 2	0.438e − 2	0.152e − 8
Step 5	0.250e + 8	0.173e + 5	0.950e + 2	0.168e − 1	0.537e − 6	0.752e − 8
Step 9	0.692e + 8	0.127e + 5	0.408e + 2	0.241e − 2	0.119e − 6	...
Step 13	0.136e + 9	0.951e + 4	0.192e + 2	0.142e − 2	0.112e − 6	...
Step 15	0.177e + 9	0.838e + 4	0.138e + 2	0.114e − 2	0.153e − 6	...

5.3.2 Finite expansion of a thick-wall cylinder

We consider an internally pressurized thick-wall cylinder with an initial inner radius of 10, exhibiting rigid-perfectly plastic behavior with a von Mises yield condition. The material constants are selected as $K = 40\,000$ MPa, $\mu = 3800$ MPa, $Y_0 = Y_\infty = 0.5$ MPa, and $\zeta = 0$ MPa. Since the radius of the yield surface is very small in comparison with the shear modulus one has negligible elastic deformations. A time step of 5 units is adopted in the computation so that 50% strain increment is applied at each time step. The exact solutions is available in, Prager and Hodge [1951, p. 118]. The results of the numerical experiment and the analytic solution are shown in Figs. 8 and 9. Excellent agreement is found between analytic and computed solutions. A quadratic rate of asymptotic convergence is attained in the Newton iteration as is apparent from the results collected in Tables 3–5.

5.3.3 Finite expansion of a thick-wall hollow sphere

The material behavior is assumed to be rigid-plastic with nonlinear isotropic hardening of the saturation type. The finite element mesh corresponding to a thick-wall hollow sphere with inner and outer radius 12.5 m and 20 m is shown in Fig. 10. The material constants are selected as $K = 800$ MPa, $\mu = 300$ MPa, $Y_0 = 0.083$ MPa, $Y_\infty = 0.486$ MPa, $\delta = 0.75$, and $\zeta = 0$. The deformation mesh corresponding to 56% porosity and the computed pressure/inner radius response are shown in Figs. 11 and 12. Furthermore, the σ_{22} stress and the Mises equivalent stress[2] contours are shown in Figs. 13 and 14.

5.3.4 Finite upsetting of an axisymmetric billet

This problem was proposed as a severe test problem for finite deformation plasticity within the context of finite element method (Taylor and Becker 1983). The billet is of 10 mm radius and 30 mm height, see Fig. 15 for a plot of the finite element mesh. The objective is to achieve 64% deformation in compression. The material properties in the saturation hardening law (5.1) are selected as $K = 166.67$ MPa, $\mu = 76.92$ MPa, $Y_0 = Y_\infty = 0.7$ MPa, and $\zeta = 0.3$ MPa. The total number of time steps is 120 and the deformed mesh corresponding to 64% is shown in Fig. 16. For comparison with the results reported in Taylor and Becker (1983), we present the Mises equivalent

2 The Mises equivalent stress is deinfed $\sqrt{\frac{3}{2}}\,\|\mathrm{dev}\,\tau\|$

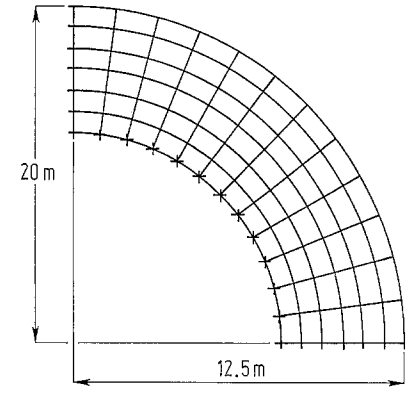

10

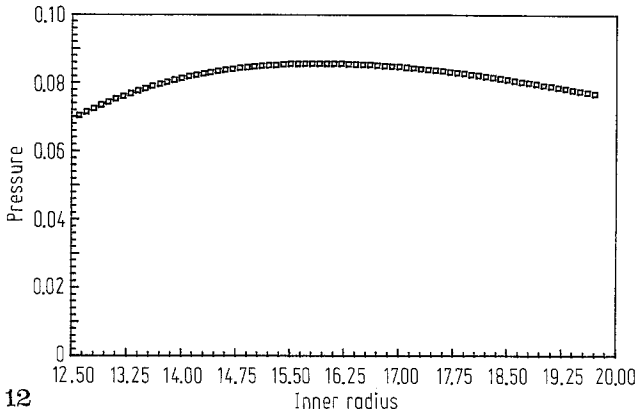

12

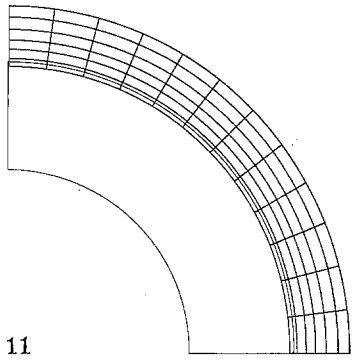

11

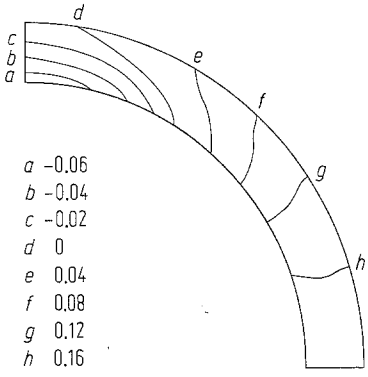

13

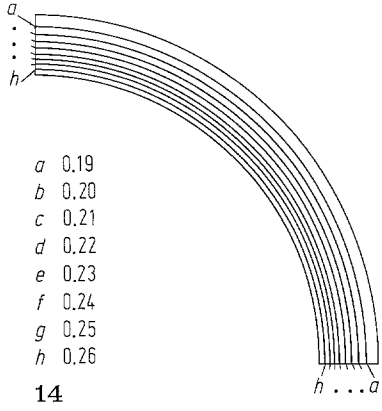

14

Figs. 10–14. Internal expansion of a thick hollow sphere; **10** finite element mesh (1/4), bilinear quadrilateral elements with constant pressure and constant Jacobian; **11** the deformation mesh corresponding to 56% porosity; **12** internal pressure vs. inner radius response curve; **13** σ_{22} stress contours a: -0.06, b: -0.04, c: -0.02, d: 0.00, e: 0.04, f: 0.08, g: 0.12, h: 0.16; **14** Mises equivalent stress contours a: 0.19, b: 0.20, c: 0.21, d: 0.22, e: 0.23, f: 0.24, g: 0.25, h: 0.26

stress contour and the load-deflection curve in Figs. 17 and 18, respectively. The jump in the load-deflection curve is due to the contact algorithm employed.

5.3.5 Finie upsetting of an axisymmetric disk

This upsetting problem was originally considered in Nagtegaal and de Jong (1981 a), and subsequently in Taylor and Becker (1983). The example is similar to the one discussed in the previous section. However, it represents a more severe test due to the small value of the ratio heigth/width that in high confinement of the material. The numerical values of the material parameters are as in Nagtegaal and de Jong (1981 a); i.e., $K = 833.333$ MPa, $\mu = 384.6154$ MPa, $Y_0 = Y_\infty = 1$ MPa, and $\zeta = 3$ MPa. The finite element mesh is shown in Fig. 19. The final deformed shape of the disk

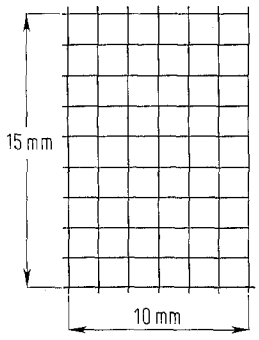

15

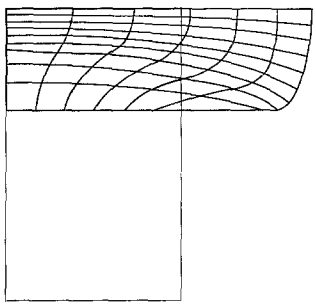

16

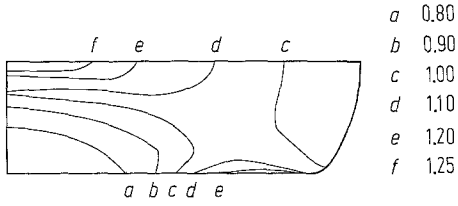

17

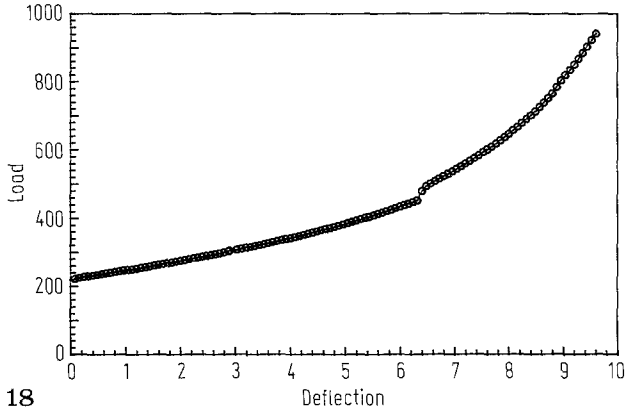

18

Figs. 15–18. Finite upsetting of an axisymmetric billet; **15** finite element mehs (1/4); **16** 64% deformation mesh; **17** Mises equivalent stress contours; **18** the global laod-deflection

corresponding to 26.67% compression is attained in 100 equal time steps, and is shown in Fig. 20. The Mises equivalent stress contours and the load-deflection curve are presented in Figs. 21 and 22, respectively. The computed load deflection curve is in excellent agreement with the results reported by Nagtegaal and de Jong (1981 a) for the 4-nooded constant dilatation element. The results reported by Taylor and Becker (1983), on the other hand, are slightly stiffer.

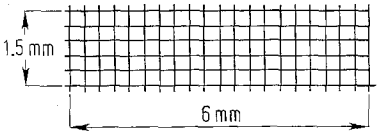

19

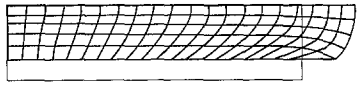

20

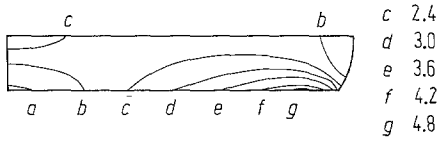

21

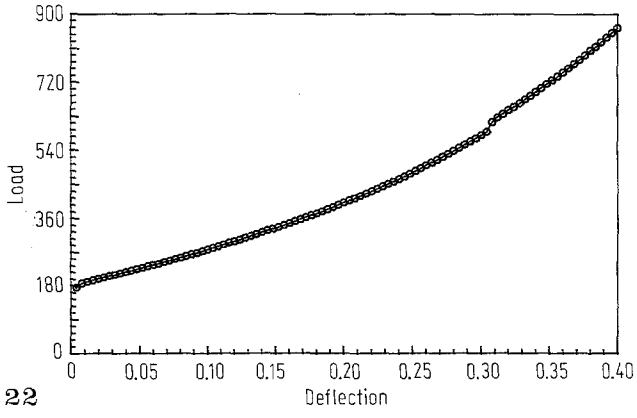

22

Figs. 19–22. Finite upsetting of an axisymmetric disk; **19** finite element mesh (1/4), bilinear quadrilateral elements with constant pressure and constant Jacobian; **20** 26.67% deformation mesh; **21** Mises equivalent stress contours; **22** the global load-deflection

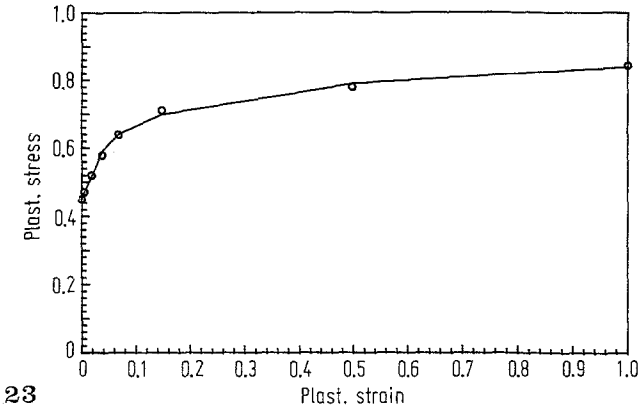

23

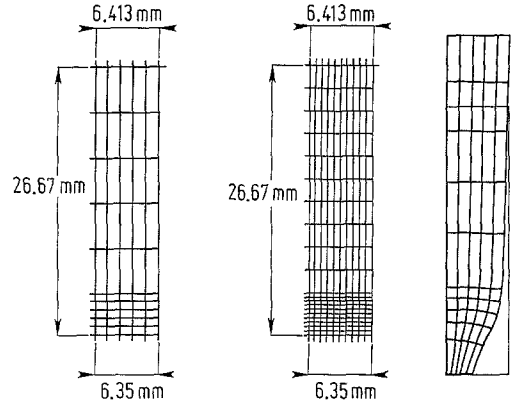

24

25

26

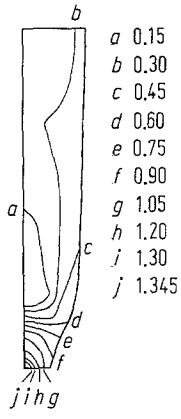

27

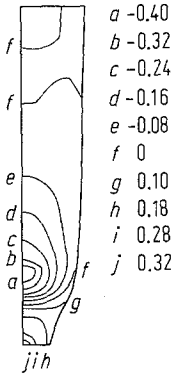

28

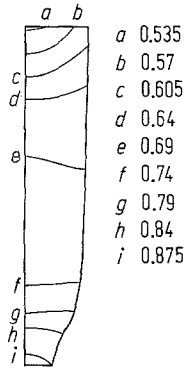

29

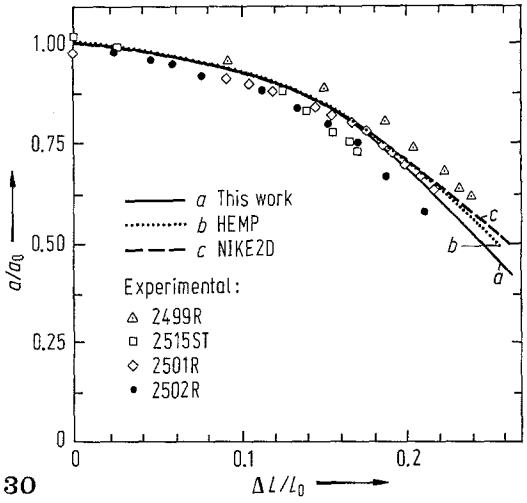

30

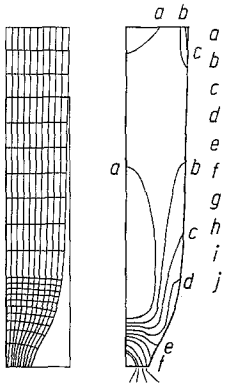

31

32

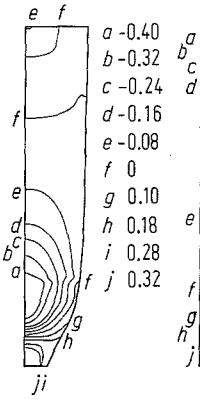

33

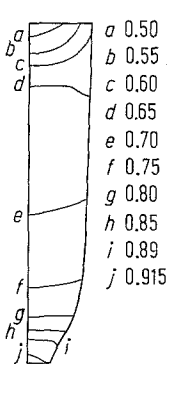

34

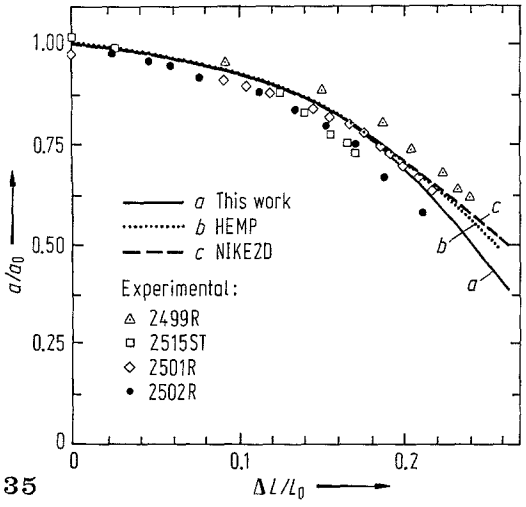

35

Figs. 23–35 Necking of a circular bar; **23** fitting of the isotropic hardening data with exponential hardening law; **24** finite element mesh (1/4) with 50 4-node quadrilateral elements; **25** finite element model with 200 4-node quadrilateral elements; **26** deformed shape at $\Delta L = 14$ mm for 50-element mesh; **27** the longitudinal (σ_{22}) stress contours for 50-element mesh; **28** the lateral (σ_{11}) stress contours for 50-element mesh; **29** the Mises equivalent stress contours for 50-element mesh; **30** neck radius versu elongation for 50.8 mm gauge length, 50-element mehs; **31** deformed shape at $\Delta L = 14$ mm for 200-element mesh; **32** the longitudinal (σ_{22}) stress contours for 200-element mesh; **33** the lateral (σ_{11}) stress contours for 200-element mesh; **34** the Mises equivalent stress contours for 200-element; **35** neck radius versus elongation for 50.8 mm gauge length. 200-element mesh

5.3.6 Necking of a circular bar

This problem poses the most severe test to the elastoplastic formulation proposed due to its high sensitivity. The problem was first proposed by Norris (1976) and is considered in Hallquist (1983). The bulk and shear moduli were taken as 164.206 GPa and 80.1938 GPa, respectively. The hardening data is fitted with the nonlinear isotropic hardening law (5.1) (Fig. 23) leading to the following values of the material parameters: $Y_0 = 0.45$ GPa, $Y_\infty = 0.715$ GPa, $\delta = 16.93$, and $\zeta = 0.12924$ GPa.

We present numerical simulations corresponding to two different finite element meshes consisting of 50 elements and 200 elements, respectively, shown in Figs. 24 and 25. The deformed shape at $\Delta L = 14$ mm for the case of 50-element mesh is shown in Fig. 26. Figures 27 and 28 show the longitudinal (σ_{22}) and lateral (σ_{11}) stress contours, respectively. The Mises equivalent stress contours are shown in Fig. 29. The ratio of the current neck radius over the initial neck radius (a/a_0) is plotted against the change in length over the initial length ($\Delta L/L_0$) in Fig. 30. This figure also includes a comparison with experimental results, as well as with numerical solutions obtained with the HEMP code (Giroux 1973) in 29,000 load increments, and NIKE2D (Hallquist 1983) in 100 times steps. The computed solution – obtained with 25 boundary displacement increments for the 50-element mesh and 53 displacement increments for the 200-element mesh – is softer than the HEMP and NIKE2D calculations. Figures 31–35 show the numerical results corresponding to the 200-element mesh. As expected, the results for the 200-element mesh are smoother and exhibit a more pronounced necking pattern than those corresponding to the 50-elements mesh.

This example proved to be a far more demanding test than any of the other simulation previously considered, as illustrated the following two qualitative aspects:

(i) The proposed approach, although not intended for problems involving very large strains, does capture accurately the correct solution even in the presence of large strains.

(ii) It appears, however, that numerical ill-conditioning tends to increase with increasing magnitude of the strains. This simulation is a case in point. The calculation with 200 element mesh could not be completed successfully in 25 time steps. Even for 100 load steps special care needed to be exercised for load levels in the neighborhood of 90% of the final displacement.

6 Conclusions

A computational framework for finite strain damage-elastoplasticity model featuring the split of the stress tensor has been presentend, and its algorithmic treatment discussed in detail. The proposed approach does offer a very convenient framework for the development of continuum damage models which can accommodate an alternative characterization of finite deformation plasticity that does not rely on the introduction at the outset of an intermediate configuration. From a computational viewpoint the simplicity of the algorithmic treatment of damage degradation renders the proposed framework specially well suited for large scale inelastic calculations. This feature has been illustrated in the numerical simulations presented.

Our alternative characterization of plasticity has some noteworthy features. In particular, the hyperelastic formulation of J_2-flow theory includes a rate free generalization of the Prager-Ziegler hardening law which is free from spurious stress-oscillations. In the simple shear test with pure kinematic hardening, for instance, this hardening law results in a linear relation between true shear stress and amount of shear.

The general applicability of the proposed approach is illustrated by the examples presented in Sect. 5. These simulations range from comparisons with exact available homogeneous solutions, to a variety of boundary value problems including elastic-damage, coupled elastoplastic-damage, as well as upsetting and necking problems.

Strain-softening response is a main issue that has not been addressed in this paper, and requires further research. The numerical simulation considered in Sect. 5.2, nevertheless, did not exhibit significant mesh sensitivity. There are several ways in which strain-softening control mechanisms can be accommodated within the present framework and that further research will address:

(1) The viscous-damage regularization discussed in Remark 2.3 and Remark 4.2. The results reported in Sandler and Wright (1984) appear to indicate that a viscous regularization leads to a well-posed initial-value problem when ellipticity fails in the rate independent case.

(2) A non-local damage evolution governing the damage variable d. This is a promising approach recently considered in Bazant and Belytschko (1987).

(3) Modification of the softening parameters along the lines advocated by Pietruszczak and Mroz (1981) and William (1987).

Appendix A: Derivation of consistent elastoplastic tangent modulus

The closed form expression for the consistent deviatoric elastoplastic tangent modulus given in Box 5 is derived concisely in this Appendix. Let us start by recalling the definition of trial elastic deviatoric stres:

$$\mathbf{s}_{n+1}^{\text{trial}} := J^{-2/3}\,\text{dev}\,[\mu\,\mathbf{b}_{n+1} - \mathbf{F}_{\mathbf{u}}\,\mathbf{s}_n^p\,\mathbf{F}_{\mathbf{u}}^T] \tag{A.1}$$

By taking the derivative of (A.1) with respect to $\mathbf{g}$ and multiplying two, we obtain the following trial elastic deviatoric tangent modulus

$$\mathbf{a}_{\text{dev}n+1}^{\text{trial}} := \frac{2}{3}\,I_{n+1}^{\text{trial}}\left[\boldsymbol{I} - \frac{1}{3}\,\mathbf{g}\otimes\mathbf{g}\right] - \frac{2}{3}\,[\mathbf{s}_{n+1}^{\text{trial}}\otimes\mathbf{g} + \mathbf{g}\otimes\mathbf{s}_{n+1}^{\text{trial}}] \tag{A.2}$$

where I_{n+1}^{trial} is defined as

$$I_{n+1}^{\text{trial}} := \mu\,\text{tr}\,\bar{\mathbf{b}}_{n+1} - \text{tr}\,[\bar{\mathbf{F}}_{\mathbf{u}}\,\mathbf{s}_n^p\,\bar{\mathbf{F}}_{\mathbf{u}}] \tag{A.3}$$

Hence we have

$$\mathbf{a}_{n+1}^{\text{trial}} : \mathbf{n} = \frac{2}{3}\,[I_{n+1}^{\text{trial}}\,\mathbf{n} - \|\mathbf{s}_{n+1}^{\text{trial}}\|\,\mathbf{g}] \tag{A.4}$$

in which $\mathbf{n}$ is defined in (3.7).
Referring to (3.6c) and take derivative with respect to $\mathbf{g}$, we obtain

$$\mathbf{a}_{\text{dev}n+1}^{ep} = \mathbf{a}_{\text{dev}n+1}^{\text{trial}} - 4\,\mathbf{n}\otimes\bar{\mu}\,\frac{\partial\gamma}{\partial\mathbf{g}} - 4\,\bar{\mu}\,\gamma\,\frac{\partial\mathbf{n}}{\partial\mathbf{g}} - 4\,\gamma\,\mathbf{n}\otimes\frac{\partial\bar{\mu}}{\partial\mathbf{g}} \tag{A.5}$$

For convenience, we first compute the linearization of $\|\mathbf{s}_{n+1}^{\text{trial}}\|$ $(= (s^{ij}s^{kl}g_{ik}g_{jl})^{1/2})$

$$2\,\frac{\partial\|\mathbf{s}_{n+1}^{\text{trial}}\|}{\partial\mathbf{g}} = \mathbf{a}_{\text{dev}n+1}^{\text{trial}} : \mathbf{n} + 2\|\mathbf{s}_{n+1}^{\text{trial}}\|\,\mathbf{n}^2 \tag{A.6a}$$

From (A.4) and (A.6a) we arrive that

$$2\,\frac{\partial\|\mathbf{s}_{n+1}^{\text{trial}}\|}{\partial\mathbf{g}} = \frac{2}{3}\,I_{n+1}^{\text{trial}}\,\mathbf{n} + 2\|\mathbf{s}_{n+1}^{\text{trial}}\|\left(\mathbf{n}^2 - \frac{1}{3}\,\mathbf{g}\right) \tag{A.6b}$$

Next we compute the linearization of $\mathbf{n}$ as

$$2\,\frac{\partial\mathbf{n}}{\partial\mathbf{g}} = \frac{1}{\|\mathbf{s}_{n+1}^{\text{trial}}\|}\,[\mathbf{a}_{\text{dev}n+1}^{\text{trial}} - \frac{2}{3}\,I_{n+1}^{\text{trial}}\,\mathbf{n}\otimes\mathbf{n}] + \frac{2}{3}\,\mathbf{n}\otimes\mathbf{g} - 2\,\mathbf{n}\otimes\mathbf{n}^2 \tag{A.7}$$

In addition, the linearization of $\bar{\mu}$ becomes

$$2\,\frac{\partial\bar{\mu}}{\partial\mathbf{g}} = \frac{2}{3}\,[\mu J^{-2/3}\,\text{dev}\,\bar{\mathbf{b}} - \bar{\mu}\,\mathbf{g}] \tag{A.8}$$

For the linearization of γ_{n+1}, recall that

$$\|\mathbf{s}_{n+1}^{\text{trial}}\| - 2\,\bar{\mu}\,\gamma_{n+1} = \sqrt{\frac{2}{3}}\,\varkappa\left(\bar{e}_n^p + \sqrt{\frac{2}{3}}\,\gamma_{n+1}\right) \tag{A.9}$$

The linearization of (A.9) then yields

$$4\,\bar{\mu}\,\frac{\partial\gamma}{\partial\mathbf{g}} - \frac{1}{1 - \varkappa'/3\,\bar{\mu}}\left[2\,\frac{\partial\|\mathbf{s}_{n+1}^{\text{trial}}\|}{\partial\mathbf{g}} - 4\,\gamma_{n+1}\,\frac{\partial\bar{\mu}}{\partial\mathbf{g}}\right] \tag{A.10}$$

By substituting (A.7), (A.8), (A.10) into (A.5) and collecting terms, we obtain the following non-symmetric consistent deviatoric elastoplastic tangent modulus

$$\mathbf{a}^{ep}_{\mathrm{dev}n+1} := f_0\, \mathbf{a}^{\mathrm{trial}}_{n+1} - \delta_1 \mathbf{n}\otimes\mathbf{n} - \delta_2 \mathbf{n}\otimes\mathbf{g} - \delta_3 \mathbf{n}\otimes\mathbf{n}^2 + \delta_4 \mathbf{n}\otimes \mathrm{dev}\,\bar{\mathbf{b}}_{n+1} \tag{A.11}$$

in which the ratios are defined in Box 5. Symmetrization of the above expression for the consistent tangent moduli yields

$$\mathbf{a}^{ep}_{\mathrm{dev}n+1} := f_0\, \mathbf{a}^{\mathrm{trial}}_{n+1} - \delta_1 \mathbf{n}\otimes\mathbf{n} - \delta_2 [\mathbf{n}\otimes\mathbf{g}]^s - \delta_3 [\mathbf{n}\otimes\mathbf{n}^2]^s + \delta_4 [\mathbf{n}\otimes \mathrm{dev}\,\bar{\mathbf{b}}_{n+1}]^s \tag{A.12}$$

which is the result shown in Box 5 (iii).

Acknowledgments

We are indebted to R.L. Taylor for his involvement in this work and many joint discussions. Support for this research was provided by NSF under Grant N° MSM 8657740 with Standford University, and DNA and AFOSR under grant No. AFOSR 880324 with the Princeton University. This support and the interest of Dr. E. Sevin is gratefully acknowledged.

References

Atluri, S.N.; Nishioka, T. (1985): Numerical studies in dynamic fracture mechanics. Int. Fract. 27, 245–261

Atluri, S.N.; Nishioka, T.; Nakagaki, M. (1985): Incremental path-independent integrals in inelastic and dynamic fracture mechanics. Eng. Fract. Mech. 20, 193–208

Bathe, K.J.; Cimento, A.P. (1980): Some practical procedures for the solution of nonlinear finite element equations. Comput. Methods Appl. Mech. Eng. 22, 59–85

Bathe, K.J.; Sonnad, V. (1980): On effective implicit time integration in analysis of fluid-structure problems. Int. J. Numer. Meth. Eng. 15, 943–948

Bazant, Z.P.; Belytschko, T. (1987): Strain softening continuum damage: localization and size effect. Proc. 2nd international conference on constitutive laws, University of Arizona, Tucson

Coleman, B.D.; Gurtin, M. (1967): Thermodynamics with internal variables. J. Chem. Phys. 47, 597–613

Flory, R.J. (1961): Thermodynamic relations for high elastic material. Trans. Faraday Soc. 57, 829–838

Giroux, E.D. (1973): HEMP user's manual. Lawrence Livermore Lab. Rep. UCRL-51079

Hallquist, J.O. (1983): NIKE2D – A vectorized, implicit, finite deformation, finite element code for analyzing the static and dynamic response of 2-D solids. Lawrence Livermore National Lab. rep. UCID-19677

Hughes, T.J.R. (1987): A course in linear finite elements. New York: Prentice-Hall

Kachanov, L.M. (1958): Time of the rupture process under creep conditions. Izv. Akad. Nauk, SSSR Otd. Tekh. Nauk 8, 26–31

Key, S.W. (1984): On an implementation of finite strain plasticity in transient dynamic large-deformation calculations. In Nemat-Nasser, S. (ed.), Theoretical foundation for large-scale computations for nonlinear material behavior Amsterdam: Nijhoff

Knott, J.F. (1973): Fundamentals of fracture mechanics. London: Butterworth

Krieg, R.D.; Krieg, D.B. (1977): Accuracies of numerical solution methods for the elastic-perfectly plastic model. J. Press. Vessel Tech. 99, 510–515

Lemaitre, J. (1984): How to use damage mechanics. Nucl. Eng. Des. 80, 233–245

Levenberg, K. (1944): A method for the solution of certain non-linear problems in least squares. Quart. Appl. Math. 2, 164–168

Luenberger, D.G. (1984): Introduction to linear and nonlinear programming, 2nd edn. New York: Addison-Wesley

Marquardt, D.W. (1983): An algorithm for the least-square estimation of nonlinear parameters. J. SIAM 11, 431–441

Marsden, J.E.; Hughes, T.J.R. (1983): Mathematical foundations of elasticity. Englewood Cliffs/Prentice-Hall

Matthies, H.; Strang, G. (1979): The solution of nonlinear finite element equations. Int. J. Numer. Math. Eng. 14, 1613–1626

Mazars, J. (1982): Mechanical damage and fracture of conrete structures. Adv. Frac. Res. 4, 1499–1506

Pietruszczak, S.; Mroz, Z. (1981): Finite element analysis of deformation of strain-softening materials. Int. J. Numer. Meth. Eng. 17, 327–334

Nagtegaal, J.C.; de Jong, J.E. (1981a): Some computational aspects of elastic-plastic large strain analysis. Int. Numer. Meth. Eng. 17, 15–41

Nagtegaal, J.C.; de Jong, J.E. (1981b): Some aspects of non-isotropic work-hardening in finite strain plasticity. In: Lee, E.H.; Mallett, R.L. (eds.) Plasticity of metals at finite strain, pp. 65–102. Proc. research workshop, Stanford University

Norris, D.M.Jr (1976): Private communication. Lawrence Livermore Lab.

Norris, D.M.Jr.; Moran, B.; Scudder, J.K.; Quinones, D.F. (1978): A computer simulation of the tension test. J. Mech. Phys. Solids 26, 1–19

Ortiz, M. (1985): A constitutive theory for the inelastic behavior of concrete. Mech. Mater. 4, 67–93

Ortiz, M.; Simo, J.C. (1986): An analysis of a new class of integration algorithms for elastoplastic constitutive relations. Int. J. Numer. Meth. Eng. 23, 353–366

Pazy, (1983): Semigroups of linear operators and applications to partial differential equations. Berlin, Heidelberg, New York: Springer (Applied Mathematical Sciences, vol. 44)

Prager, W.; Hodge, P.G. (1951): Theory of perfectly plastic solids. New York: Wiley

Sandler, I.; Wright, J. (1984): Summary of strain-softening. In. Nemat-Nasser, S. (ed.) Theoretical foundation for large scale computations of nonlinear material behavior. DARPA-NSF Workshop, Northwestern University

Simo, J.C. (1987a): On a fully three-dimensional visco-elasticity damage model: formulation and computational aspects. Comput. Methods Appl. Mech. Eng. 60, 153–173

Simo, J.C. (1988b, c): A framework for finite strain elastoplasticity based on maximum plastic dissipation and the multiplicative decomposition: computational aspects. Part II. Comput. Methods Appl. Mech. Eng. 68, 1–31

Simo, J.C.; Ju J.W. (1987a): Strain and stress based contunuum damage models. I: Formulation. Int. J. Solids Structures 23, No. 7, 821–840

Simo, J.C.; Ju, J.W. (1987b): Strain and stress based continuum damage models. II: Comptational aspects. Int. J. Solids Structures, 23, 7, 841–869

Simo, J.C.; Marsden, J.E. (1984): On the rotated stress tensor and the material version of the Doyle-Erickson formula. Arch. Rat. Mech. Anal. 86, 213–231

Simo, J.C.; Ortiz, M. (1985): A unified approach to finite deformation elastoplasticity based on the use of hyperelasic relations. Comput. Methods Appl. Mech. Eng. 49, 221–245

Simo, J.C.; Taylor, R.L. (1985): Consistent tangent operators for rate independent elasto-plasticity. Comput. Methods Appl. Mech. Eng. 48, 101–118

Simo, J.C.; Taylor, R.L.; Pister, K.S. (1985): Variational and projection methods for the volume constraint in finite deformation elasto-plasticity. Comput. Methods Appl. Mech. Eng. 51, 177–208

Taylor, L.M.; Becker, E.B. (1983): Some computational aspects of large deformation, rate-dependent plasticity problems. Comput. Methods Appl. Mech. Eng. 41, 251–277

Wilkins, M.L. (1964): Calculation of elastic-plastic flow. Methods Comput. Phys. 3

Willam, K.; Prameno, E.; Sture, S. (1987): Uniqueness and stability issues of strain softening computations. Proc. 2nd international conference on constitutive laws. University of Arizona, Tucson

Communicated by S.N. Atluri, June 8, 1988